Characterizing coastal aquifer heterogeneity from a single piezometer head chronicle

Martin Le Mesnil, Alexandre Gauvain, Frédéric Gresselin, Luc Aquilina, Jean-Raynald de Dreuzy

Journal Pre-proofs

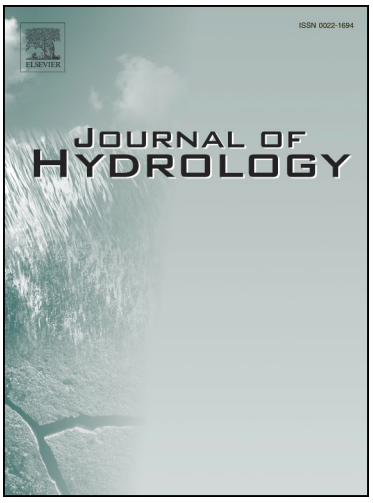

Characterizing coastal aquifer heterogeneity from a single piezometer head chronicle

Martin Le Mesnil, Alexandre Gauvain, Frédéric Gresselin, Luc Aquilina, Jean-Raynald de Dreuzy

PII: S0022-1694(24)01255-1
DOI: https://doi.org/10.1016/j.jhydrol.2024.131859
Reference: HYDROL 131859

To appear in: *Journal of Hydrology*

Please cite this article as: Le Mesnil, M., Gauvain, A., Gresselin, F., Aquilina, L., de Dreuzy, J-R., Characterizing coastal aquifer heterogeneity from a single piezometer head chronicle, *Journal of Hydrology* (2024), doi: https://doi.org/10.1016/j.jhydrol.2024.131859

Characterizing coastal aquifer heterogeneity from a single piezometer head chronicle

Martin Le Mesnil[1*], Alexandre Gauvain[2], Frédéric Gresselin[3], Luc Aquilina[1], Jean-Raynald de Dreuzy[1]

[1] Univ Rennes, CNRS, Géosciences Rennes - UMR 6118, F-35000 Rennes, France

[2] Sorbonne Université, CNRS, Laboratoire de Météorologie Dynamique, F-75005 Paris, France

[3] DREAL Normandie, Caen, France

[*]Corresponding author: martin.le-mesnil@univ-rennes.fr – Géosciences Rennes, 263 av. Général Leclerc, 35042 Rennes

Keywords: Coastal aquifer, Heterogeneous aquifer, Hydraulic head time series, Seepage, Specific yield, Hydraulic conductivity

1. Introduction

Climate change exerts particularly strong effects on coastal areas (Richardson et al., 2024). In this context, our focus is specifically on the risks associated with rising aquifer levels (Rotzoll and Fletcher, 2013). With sea levels rising by a few millimeters to a few centimeters per year depending on climate change scenarios (Rignot et al., 2011), the levels of coastal aquifer are also increasing. This poses a threat to buried and low-lying infrastructures, nearshore ecosystems, and amplifies the risk of flooding (Habel et al., 2017; Knott et al., 2017). Fluctuations in aquifer level traduce the variations of is groundwater storage, and consequently the difference between recharge and discharge. For this reason, varying seasonal rainfall and evaporation can lead to temporary increased or decreased aquifer levels, depending on discharge conditions. Both marine and continental forcings, as well as the geometry of the coastline, distance from the coast, geologic depositional environments, and regional stream network contribute to groundwater-induced flood-risk evolution in coastal areas (Knott et al., 2019). Aquifer hydraulic properties were found to be a dominant factor in groundwater-rise vulnerability, with propagation projection of 10 km from the coast and main rivers in Netherlands (Oude Essink et al., 2010).

Diffusive aquifers extend the zone of tidal influence and their associated high levels (Jacob, 1950; Nielsen, 1990). They also moderate the influence of recharge, with reduced head gradients and limited aquifer levels. Conversely, less diffusive aquifers mitigate marine influences but increase the vulnerability to groundwater rise from the continental side. This initial qualitative analysis becomes significantly more complex for heterogeneous aquifers. This is particularly true for coastal areas where Quaternary sand deposits next to the shoreface separate inland less diffusive bedrock formations from marine boundaries, a common configuration found in coastal areas like on the Western Normandy coast (France) (Dupret et al., 1989). The dune ridge shields the adjacent low-lying area from most of the marine submersion risks but does not protect it from increasing groundwater levels. A few hundred meters to a few kilometers away inland, the bedrock rises significantly, protecting more distant coastal areas from any marine risk, but increasing the vulnerability to flooding induced by aquifer outlets.

To assess vulnerability to groundwater-induced flooding, one of the major challenges lies in characterizing hydraulic properties and their heterogeneity. Information derived from the aquifer's response to the tidal signal has been widely employed to determine these properties (e.g. Aguila et al., 2023; Fischer et al., 2020; Goyetche et al., 2022; Jha et al., 2008; Slooten et al., 2010; Zhang et al., 2021). They provide basic to advanced constraints on aquifer properties and flow structures (Rogers

et al., 2023). For homogeneous aquifers, piezometric tidal effects decrease exponentially with shore distance as a function of diffusivity (Ferris, 1952). Diffusivity can thus be determined by comparing the amplitude of piezometric head variations with that of tides (Carr and Vanderka, 1969; Slooten et al., 2010) and, for greater precision, by analyzing both signals together (Jha et al., 2008). Heterogeneous aquifers also exhibit spatial variations with hydraulic conductivity increasing linearly with the distance from the coastline in some cases (Monachesi and Guarracino, 2011), or vertically in other cases (Li and Jiao, 2003). Mapping these variations in diffusivity often requires several monitoring wells (Carol et al., 2009; Rogers et al., 2023; Yang et al., 2021). A review of methods also emphasizes the necessity to develop original approaches to independently estimate hydraulic conductivity and specific yield for water resources management (Zhang et al., 2021).

Here, we propose an alternative and innovative approach to characterize subsurface hydraulic properties (hydraulic conductivity and specific yield) and their heterogeneity, based on hydraulic head measured on a single piezometer. The method uses three aspects of aquifer response to marine and continental forcings: i) average head, which filters out the temporal variability and is linked to average recharge, sea level and hydraulic conductivity; ii) high-frequency head variations linked to tidal effects; iii) seasonal variations, which respond to hydrological cycle of aquifer recharge and discharge. We propose to characterize heterogeneous subsurface hydrodynamic properties by analyzing these three piezometric signal components, associated to characteristic time scales of weeks (spring and neap tides), months (hydrological cycle) and years (average recharge). We show that coastal aquifers may respond specifically to each of those forcings using data obtained on a coastal aquifer in Normandy, France (section 2). We propose a step-by-step approach to constrain the subsurface hydraulic properties relying on analytical and simplified 1D numerical models without considering any groundwater seepage (section 3). We compare the results obtained with a more advanced 2D numerical model, investigate the effects of seepage and of the distance of the observation piezometer to the lithological interface (section 4). We then discuss the most adapted identification method depending on the encountered conditions, and its domain of applicability. We eventually illustrate our methodology by presenting an application to groundwater-induced flooding in the studied coastal area (section 5). We believe that this is one of the key applications of our methodology, as this latter has to be applied to coastal areas, which are often prone to groundwater flooding as water table is likely to be shallow in such contexts.

2. Response of coastal hydraulic heads to tidal and recharge variations

Starting from a classic coastal context (2.1), we demonstrate the dual influence of continental and marine forcings on hydraulic head variations (2.2) and propose a quantification of their main characteristics (2.3).

2.1. Geological and hydrogeological contexts

The study area is a coastal site located in the south-western part of the town of Gouville-sur-Mer, in western Normandy, France (Figure 1, insert). It is located in the downstream part of the Moulin-de-Gouville river catchment, the source of which lies 10 km to the East. The modelled area is 1 km wide and 3.3 km long (frame in Figure 2). This site is representative of coastal areas made up of a dune ridge, a retro-littoral palaeo-cliff and, between these two groups, a sea-marsh. The palaeo-cliffs of Normandy are polygenic structures, whose formation began in the Neogene (Pedoja et al., 2018). They contain different levels of marine terraces, most often masked by periglacial cover (Bigot, 1897; Coutard et al., 2006; Elhaï, 1960; Lautridou, 1989). The most recent of these terraces is the Eemian (124,000 to 119,000 years ago), which is located in the basal parts of the paleo-cliffs and consists of perched fossil beaches of pebbles or sand (Dupret et al., 1989). Within the studied site, the dune belt reaches a

maximum elevation of 20 m. To the West, it overlooks a sea marsh, whose elevation is close to that of the sea at high tide. The paleo-cliff has a gentle profile, a result of erosion of the last ice age. The highest points of the modelled area, located to the East of the paleo-cliff, reach approximatively 25 m above sea level. Note that all elevation including hydraulic head are referenced as meters above sea level shortened as "m".

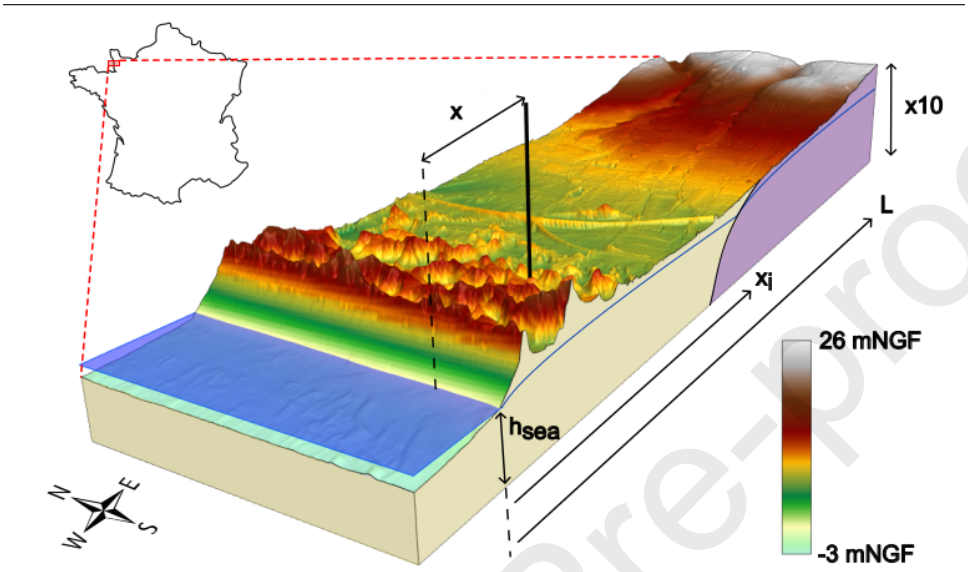

Figure 1: Topography and location of the study site within the Moulin-de-Gouville River watershed (Normandy, France).

The study site is located in a complex geological context, both from a lithological and structural point of view. It is located in the heart of the Cadomian island arc of Coutances (Dissler et al., 1988; Dupret et al., 1990), whose main geological formations are of magmatic origin (Dupret et al., 1987; Dupret et al., 1989). In the environment of the site, sedimentary formations of detrital origin are also present, of lower and upper Brioverian age. Some Cambrian sandstones also crop out to the north and on the rocky flat off the site, on the foreshore.

The geological bedrock at the study site is covered by more or less ancient Quaternary rocks, generally sandy (zone 1 in Figure 2). They are of continental or marine origin depending on the case. Under the dunes, the bedrock was reached by various drillings at a height of around ten meters. This Brioverian bedrock outcrops on the foreshore and in the paleocliff (zone 2 in Figure 2). The description of the rocks reached by the drilling does not make it possible to precisely characterize the composition of the bedrock located under the dunes, in the vicinity of the study site. Understanding its structure in detail would require high-precision geophysics coupled with close-up surveys. Nevertheless, this environment is that of a strongly faulted site. It is likely that the paleocliff originated from the presence of these structural discontinuities. The lithological differences observed between the rocks outcropping on the foreshore or in the paleocliff can only be conceived in the presence of a bundle of faults and folds masked by the dune massif and the sea marshes which border itat the foot of the paleocliff.

Figure 2 synthetizes the site geological setup, with a well-marked heterogeneity characterized by two juxtaposed distinct formations. In the western part (zone 1 on Figure 2), the site consists of recent,

loose rocks, mainly marine and eolian sands, up to 10 m thick. These sands are partially interbedded with solifluction deposits or sandy clay peat. They are referred to as Quaternary sands in the next sections. In the eastern part, the outcropping rocks (zone 2 on Figure 2) belong to the local Cadomo-Variscan bedrock (Brioverian sequence). They are designated as Brioverian shales in the next sections. They consist of variably metamorphosed sandstone and shale, as well as granite, showing fissures and surface alteration. This bedrock forms the basement of the unconsolidated rocks in the western part of the site. There is no clear discontinuity or impervious layer between the ancient rocks and the overlaying unconsolidated formations, due to a weathering layer affecting the upper part of the bedrock. It is therefore not possible to clearly distinguish an upper aquifer from a lower, confined aquifer. As a whole, the aquifer extends to a thickness of over 35 meters.

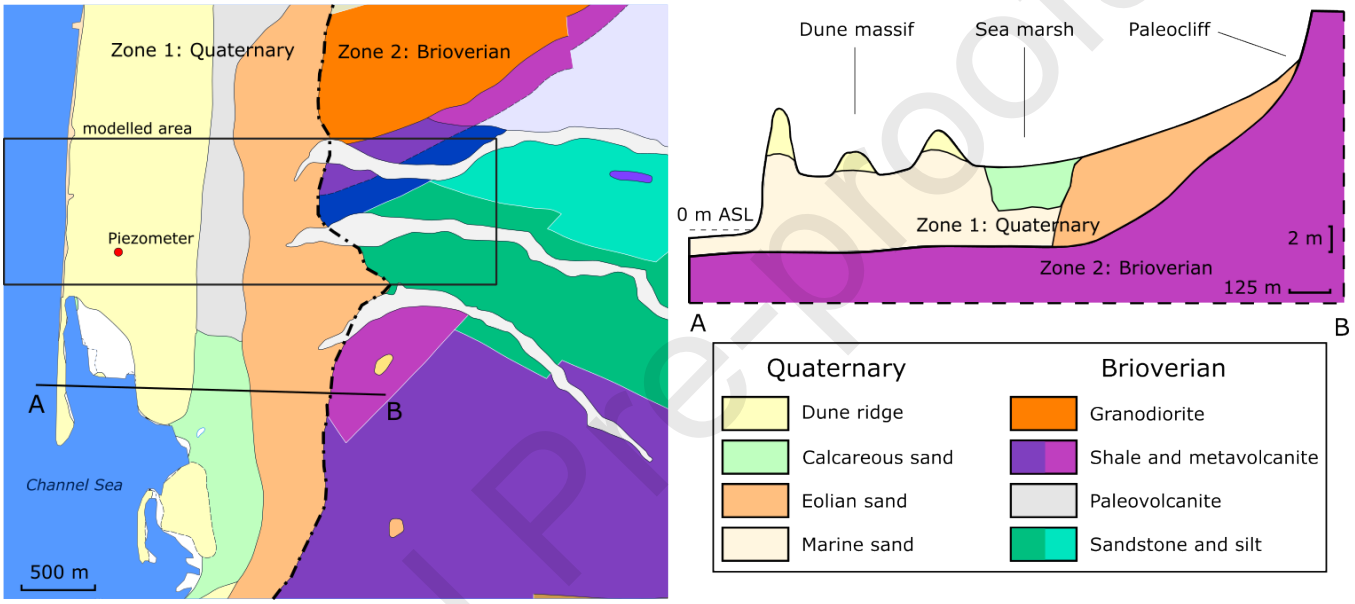

Figure 2: Modelled area, geological map (left) and simplified geological cross-section (right). Modified from Dupret et al. (1989).

2.2. Piezometric, sea-level and recharge data

The Gouville piezometer (red circle on Figure 2) has been monitored at a daily frequency since 2005. It is part of the French national network of groundwater measurements, whose information is accessible online on the ADES database (Winckel et al., 2022). The piezometer is 11 metres deep, drilled through sands within the Quaternary formation, and located 420 metres east of the shoreline. The recorded head data is shown in dark blue on Figure 3 for the 2009-2017 period. It reacts to both spring-and-neap tide and seasonal recharge forcings.

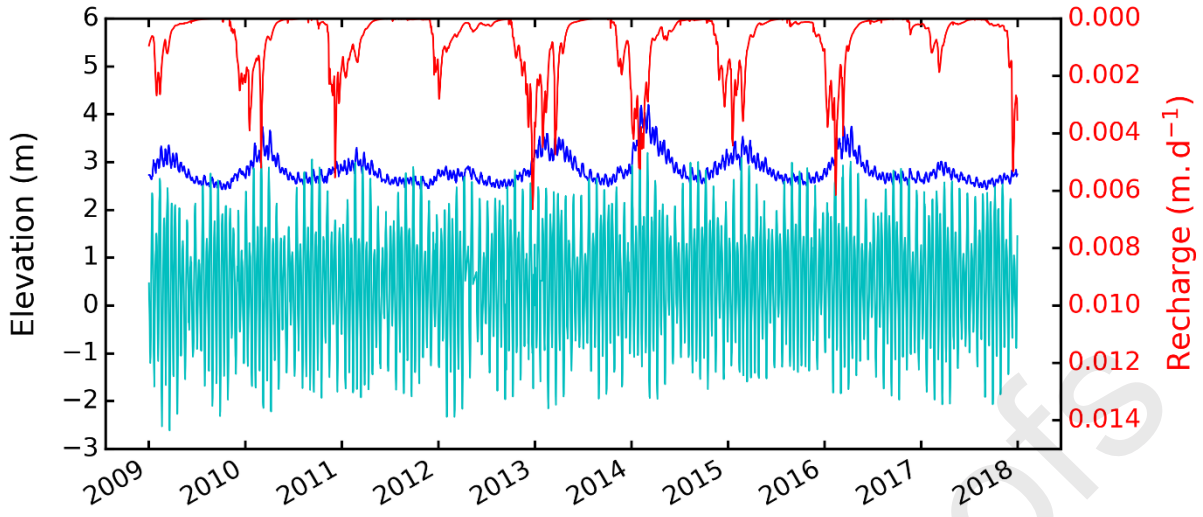

Figure 3: Read on the left axis, daily hydraulic heads in dark blue recorded at the Gouville piezometer and daily sea levels at the nearby Saint-Malo station in light blue. Read on the right axis, aquifer recharge of the modelled area in red as given by the SURFEX national climate time series (Le Moigne et al., 2020).

The high frequency variations of the head data are to compare with the tidal signal (light blue curve on Figure 3). It is obtained from the nearest oceanographic station of Saint-Malo operated by the Hydrographic and Oceanographic Marine Service, which produces oceanographic data at several coastal stations along the French shore (SHOM, 2020). Hourly levels were translated in daily levels to focus on the bimonthly tidal fluctuations, which are the only ones observed in the piezometric data. The high frequency variations of head data (dark blue) are well marked and have logically a significantly smaller amplitude than the sea level ones (light blue).

The lower frequency variations of head data are well phased with aquifer recharge (red curve on Figure 3), obtained from the SURFEX national climate model (Le Moigne et al., 2020), produced by the French meteorological institute. In SURFEX, aquifer recharge values are resulting from the exchanges of mass and energy between the soil, the surface, the biosphere and the atmosphere accounting for the wide diversity of surfaces.

2.3. Main characteristics of the hydraulic head signal

The head data display three main components: the mean pluriannual value, the amplitude of seasonal recharge-induced variation, and the amplitude of weekly tidal variations. In order to identify aquifer hydraulic properties based on these three components, we derive them from the head signal as follows:

$$h(\boldsymbol{x},t) = \overline{h}(\boldsymbol{x}) + h_r(\boldsymbol{x},t) + h_t(\boldsymbol{x},t) \qquad (1)$$

where $\overline{h}(\boldsymbol{x})$ is the mean hydraulic head at a distance to shoreline $\boldsymbol{x}$ within the aquifer, $h_r(\boldsymbol{x},t)$ and $h_t(\boldsymbol{x},t)$ are the head components respectively associated to seasonal (recharge-induced) and weekly (tide-induced) forcings. $\overline{h}(\boldsymbol{x})$ is defined by:

$$\overline{h}(\boldsymbol{x}) = \frac{1}{t_f - t_i}\int_{t_i}^{t_f} h(\boldsymbol{x},u)du \qquad (2)$$

where $\left[t_i,t_f\right]$ is the time interval over which the head data are available. In practice it should be one to several years. $h_r(\boldsymbol{x},t)$ is obtained by filtering out the tidal signal using a moving average over the tidal period of duration τ=28 days:

$$h_r(\boldsymbol{x},t) = \frac{1}{\tau}\int_{t-\tau/2}^{t+\tau/2}\left(h(\boldsymbol{x},u) - \overline{h}(\boldsymbol{x})\right)du. \qquad (3)$$

$h_t(\boldsymbol{x},t)$ is eventually obtained by removing the components previously determined:

$$h_t(\boldsymbol{x},t) = \overline{h(\boldsymbol{x})} + h_r(\boldsymbol{x},t) - h(\boldsymbol{x},t). \qquad (4)$$

Figure 4a shows the decomposition of the head levels of Gouville (Figure 2) in its recharge-indued and tide-induced components h_r and h_t. Figure 4b and 4c show the comparison to the SURFEX recharge rate and measured sea-level on a shorter time range. In order to ensure that the moving average method efficiently filters the tide-induced head fluctuations, we analyzed the correlation between the terms h_r and h_t on the one hand, and recharge and sea-level on the other hand. After applying a time lag of 41 (and 5) days to h_r (and h_t), we obtain a Pearson correlation coefficient value of 0.807 (and 0.804). This shows that SURFEX-derived recharge and measured sea-level explain more than 80 % of h_r and h_t terms, respectively. It also confirms that the 28-day moving average filter method does not significantly erase any seasonal recharge signal that would have a wavelength similar to that of spring and neap tide.

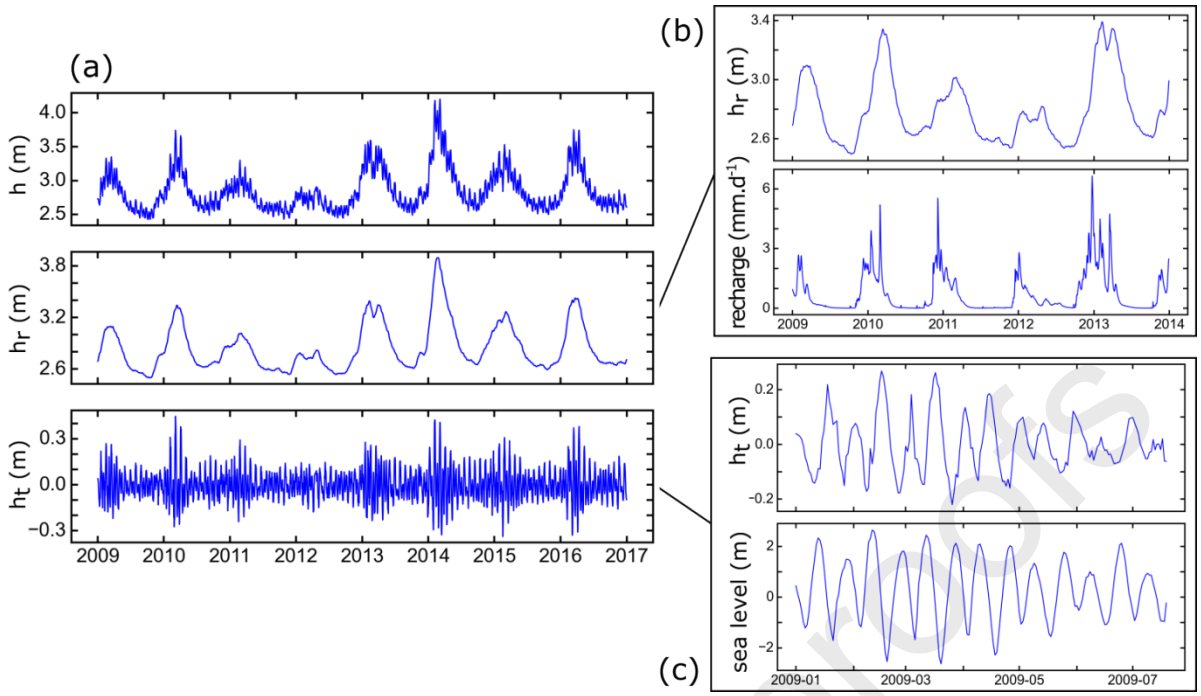

178

179 *Figure 4: (a) Time series on the 2009-2016 period of measured head h in the Gouville piezometer and*
180 *derived recharge-induced h_r and tide-induced h_t head components. (b) Time series on the 2009-2014*
181 *period of the recharge-induced head component h_r and SURFEX recharge (c) Time series on the January*
182 *to August 2009 period of the tide-induced head component h_t and measured sea-level.*

183

184 We additionally define specific model performance criteria, measuring the ability of any model to
185 match each of these components. For the mean hydraulic head, the criterion is built from the mean
186 simulated and observed heads $\overline{h^{sim}(x)}$ and $\overline{h^{obs}(x)}$:

$$\alpha = 1 - \frac{\overline{h^{sim}(x)}}{\overline{h^{obs}(x)}} \qquad (5)$$

187 The comparison of recharge- and tide-induced variations are obtained from the similar criteria β_r and
188 β_t:

$$\beta_r = 1 - \frac{\sigma_r^{sim}(x)}{\sigma_r^{obs}(x)} \qquad (6)$$

$$\beta_t = 1 - \frac{\sigma_t^{sim}(x)}{\sigma_t^{obs}(x)} \qquad (7)$$

189 where $\sigma_a^b(x)$ is the standard deviation of the head component *a*, *a* being either recharge (*r*) or tide (*t*),
190 for the simulated or observed heads (*b*=*sim* and *b*=*obs*, respectively). For the head time series of the

Gouville piezometer on the 2009-2017 period, $\overline{h^{obs}} = 2.85\ m$, $\sigma_t^{obs} = 0.12\ m$, $\sigma_r^{obs} = 0.27\ m$. Tidal fluctuations appear to be non-negligible compared to the recharge-induced variations.

3. Hydraulic properties derived with simplified analytical and numerical models

In this section, we show how the mean hydraulic head and the tidal fluctuations can be approached by analytical solutions and give a first approximation of the hydraulic properties of the Quaternary sands. We assess and complete the identification with simple 1D numerical simulations of heterogeneous free aquifers following the configuration given in section 2 and recalled in **Error! Reference source not found.**. Exploration ranges are 1 to 30 % and 10^0 to 10^3 m.d^{-1} for specific yield and hydraulic conductivity, respectively. They are determined through global synthesis (Freeze and Cherry, 1979; Gleeson et al., 2011; Rosas et al., 2014), confirmed by site-specific studies (Borehole file BSS000KUVT, 2017).

Table 1: Main site configuration and recharge metrics.

Mean aquifer extension	L	3000 m
Distance of the lithological interface to the coast	x_i	600 m
Distance of the piezometer to the coast	X	400 m
Aquifer thickness at the coast	h_{sea}	20 m
Mean recharge rate	R	286 mm.y^{-1}

3.1. Approximation of Quaternary sand hydraulic properties using analytical solutions

The mean value can be compared to the value $h(x)$ obtained at the position x from the coast in steady state for a 1D heterogeneous aquifer of size L and thickness h_{sea} at the coast, hydraulic conductivities K_1 and K_2 respectively Quaternary sand and Brioverian shale, the heterogeneity separation at a distant x_i from the coast and a homogeneous recharge R:

$$\begin{cases} 0 \le x \le x_i \quad h(x) = h_{sea}\sqrt{1 + \frac{R}{K_1}\left(\frac{L}{h_{sea}}\right)^2\left(\frac{x}{L} - \frac{1}{2}\left(\frac{x}{L}\right)^2\right)} \\ x_i \le x \le L \quad h(x) = h_{sea}\sqrt{1 + \frac{R}{K_2}\left(\frac{L}{h_{sea}}\right)^2\left(\frac{x}{L} - \frac{1}{2}\left(\frac{x}{L}\right)^2\right) + \left(\frac{R}{K_1} - \frac{R}{K_2}\right)\left(\frac{L}{h_{sea}}\right)^2\left(\frac{x_i}{L} - \frac{1}{2}\left(\frac{x_i}{L}\right)^2\right)} \end{cases} \quad (8)$$

The head, $h(x)$, logically increases from its value at the coast, h_{sea}, as a square root function of x/L, a dependence characteristic of free aquifers. In the Quaternary sands ($0 \le x \le x_i$), it does not depend

on K_2. As the aquifer is not constrained by any interactions with the surface and does not have any other outlet than the coast, the same incoming flux accumulated in the Brioverian shale $R(L\text{-}x_i)$ is transferred to the Quaternary sands, regardless of the value of K_2. K_1 can be directly estimated from the first equation of (8) as:

$$K_1 = R\,\frac{\left(\frac{L}{h_{sea}}\right)^2\left(\frac{x}{L}-\frac{1}{2}\left(\frac{x}{L}\right)^2\right)}{\left(\frac{h(x)}{h_{sea}}\right)^2-1} \tag{9}$$

leading to a first approximation of K_1=17.61 m.d^{-1} for the configuration given by**Error! Reference source not found.**. It should be noted that this value does not account for multiple important processes including the interception of the aquifer water table with the surface, the potential existence of outlets at the hydrographic network, which may be quite significant in this area downstream in the hydrological system as well as differences between mean head levels and steady state levels, which may occur because of the non-linearity of the free aquifer flow equation.

Tidal head fluctuations can be approached by the diffusion of the tidal signal within a homogeneous confined aquifer given by (Nielsen, 1990) as:

$$h(x,t) = h_{sea} + \frac{A}{2}\cos\left(2\pi\frac{t}{\tau}-\frac{x}{l_c}\right)\exp\left(\frac{-x}{l_c}\right) + \frac{R}{K_1}x \quad \text{with} \quad l_c = \sqrt{(\tau K_1 e)/(\pi S y_1)} \tag{10}$$

where A and τ are respectively the amplitude and period of the tidal forcing signal, Sy_1 is the specific yield of the Quaternary sands and e is the mean aquifer thickness.

We then use the terms of equation (10) relating to tidal wave propagation to calculate the variance of tidal fluctuations σ_t^2:

$$\sigma_t^2 = \int_0^{\tau}\left[\frac{\mathrm{A}}{2}\cos\left(2\pi\frac{\mathrm{t}}{\tau}-\frac{\mathrm{x}}{\mathrm{l_c}}\right)\right]^2\exp\left(\frac{-\mathrm{x}}{\mathrm{l_c}}\right)\mathrm{dt} \tag{11}$$

Equation (11) provides a new expression for l_c:

$$\mathrm{l_c} = \frac{\mathrm{x}}{\ln(\mathrm{A}/(2^{3/2}\sigma_\mathrm{t}))} \tag{12}$$

With the bimonthly tidal amplitude A = 5.8 m and assuming (i) that the mean aquifer thickness e is equal to h_{sea} and (ii) that it is large enough for the confined aquifer assumption to hold for the free aquifer conditions, we can derive a first approximation of the specific yield Sy_1 using expressions of l_c in both (10) and (12):

$$Sy_1 = \frac{\tau K_1 e}{\pi}\left(\frac{\ln\left(\left(A/\left(2^{3/2}\sigma_t^{obs}\right)\right)\right)}{x}\right)^2 \tag{13}$$

Where we recall that σ_t is the standard deviation of the tidal fluctuations. Using the value of K_1 previously determined, we obtain a value of Sy_1 of 10% ($Sy_1 = 0.1$). As for K_1, this approximation is subject to several assumptions. As already mentioned, the free aquifer solution should not be too far from the confined one. The Brioverian shale of different hydraulic conductivity K_2 and specific yield Sy_2 should also have a small enough influence on the diffusion of the tidal signal. We finally note that, using these first approximations, the characteristic amplitude of the bi-daily tidal signal would be of the order of 10^{-5} m, a value that cannot in fact be observed.

Using these two analytical solutions, the hydraulic properties of the Quaternary sands can be approximated under the afore mentioned assumptions. The hydraulic properties of the Brioverian shales are more difficult to assess as they will influence the seasonal head fluctuations for which, to the best of our knowledge, no analytical solution is available for heterogeneous aquifers in transient state. We thus use a simplified numerical model to constrain the hydraulic properties of the Brioverian shale (K_2, Sy_2).

247 *Table 2: Hydraulic properties obtained from the analytical, 1D and 2D numerical models.*

	Analytical	**Numerical 1D**	**Numerical 1D**	**Numerical 2D**	**Numerical 2D**	**Numerical 2D**
Distribution	Homogeneous	Homogeneous	Heterogeneous	Heterogeneous	Heterogeneous	Heterogeneous
Seepage	Not allowed	Not allowed	Not allowed	Not observed	Observed	Observed
x_i (m)	1 000	1 000	1 000	1 000	1 000	500
K_1 (m.d^{-1})	18	18	18	18	10 - 17	5.0 - 20
Sy_1 (%)	10	7.1	7.1	8.0	4.4 – 7.5	4.4 – 7.5
D_1 (m^2.d^{-1})	$3.5\ 10^3$	$5.2\ 10^3$	$5.2\ 10^3$	$4.5\ 10^3$	$2.6\ 10^3$ – $7.7\ 10^3$	$1.3\ 10^3$ – $9.0\ 10^3$
K_2 (m.d^{-1})			20 – $1.0\ 10^3$	9.0 - 30	1.0 – 8.0	1.0 - 15
Sy_2 (%)			23 - 30	27 - 30	15 – 30	10 - 15
D_2 (m^2.d^{-1})			$1.3\ 10^2$ – $8.7\ 10^4$	6.0^2 – $2.6\ 10^3$	$7.0\ 10^1$ – $7.0\ 10^2$	$7.0\ 10^1$ – $1.2\ 10^3$

3.2. Constrains on Brioverian shale hydraulic properties with a 1D numerical model

To complete the identification, we set up a simplified 1D free aquifer perpendicular to the shoreline having the same characteristic as the one presented in the previous subsection. The head is fixed at the coast by the tidal signal (Figure 3, light blue curve). The recharge applied uniformly on the top of the model is taken from the SURFEX reanalysis (Figure 3, red curve). A no-flow boundary condition is applied upstream at $x=L$ to represent the groundwater divide at the watershed limit. The minimal aquifer thickness is set at its value at the coast (h_{sea}=20 m). The free-flow model is carried out using MODFLOW NWT (Harbaugh, 2005; Niswonger et al., 2011) with 1-meter-wide mesh cells and daily time steps. The initial head values are set to the steady-state solution obtained from the mean recharge and sea level.

We first and synthetically evaluate the quality of the approximations given by the previous analytical solutions with a homogeneous numerical model with the values of K_1 and Sy_1 obtained previously by the analytical solutions. Results give values of $\alpha =$ 0.014 and $\beta_t =$ 0.013, showing indeed close agreements. Calibrating directly with the numerical model instead of the analytical solutions following the same procedure would lead to close values K_1=18.33 m.d^{-1} and Sy_1=7.1%. The relevance of the analytical solution was expected for the mean head. It is more conclusive on the confined assumption for the tidal fluctuations. Even though the homogeneous model captures well the mean head and the tide-induced signal (red curve), it remains far from the observed signal (blue curve, Figure 5). Seasonal variations are too large. For some of the later years (2013-2017), winter levels are overestimated by 0.2-0.5 meters. For the earlier years (2009-2012) and the last year 2018, summer recessions are underestimated by around half a meter. It shows that the model calibrated on the mean level and on the tidal variations displays too large seasonal variations. In other words, the response to the tidal fluctuations and the mean level imposes that the aquifer is not capacitive enough to buffer the seasonal variations of recharge shown by the observations. We provide additional details in Section 5 regarding the utilization of the earlier identification and comparison as a homogeneity test.

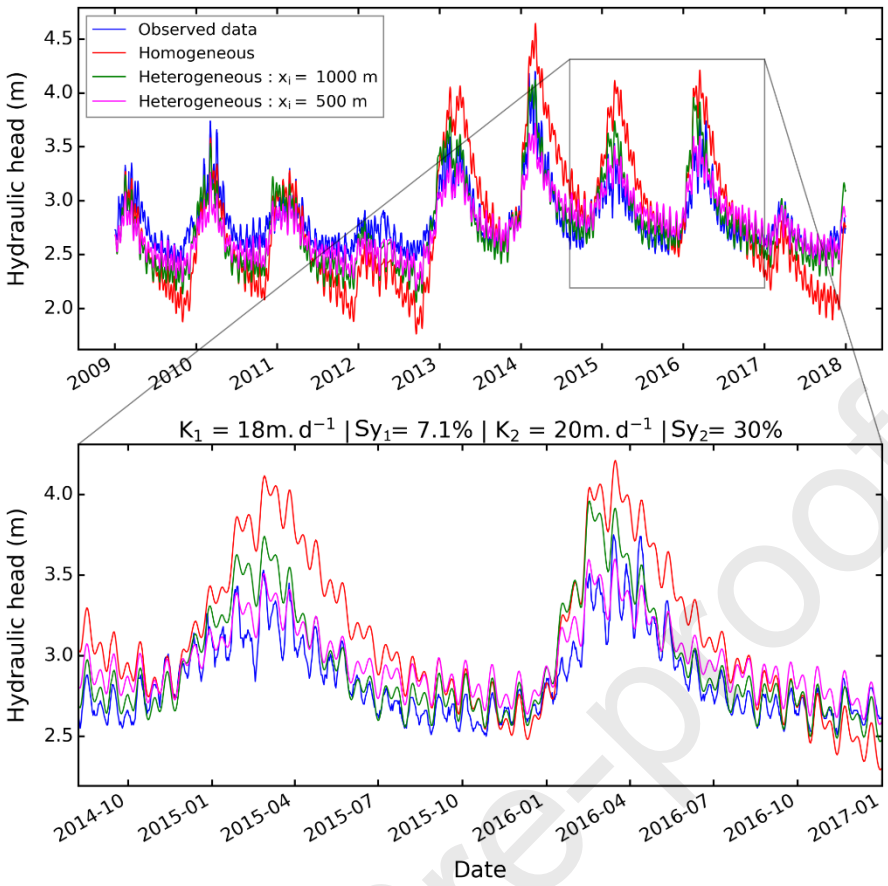

Figure 5: Comparison of the hydraulic head chronicle observed at the Gouville piezometer shown by the red point on Figure 1 (blue curve) with the results obtained by the 1D homogeneous analytical solution (red curve), the 1D heterogeneous numerical model (green curve) and the 1D heterogeneous model with the position of the interface closer at x_i=500 m (pink curve). Model parameters are given in Table 2.

We set up a heterogeneous model, derived from the homogeneous model, to accurately capture seasonal variations while maintaining the calibration of the mean hydraulic head and tidal fluctuations. To this end, we perform a sensitivity analysis of the recharge variations criterion β_r as a function of K_2 and Sy_2 at fixed values of the Quaternary sand hydraulic properties K_1 and Sy_1, those values obtained with the analytical solutions (Figure 6). The range of values of K_2 is limited to a minimum value of 20 m.d^{-1} to restrain the piezometric values below the topography and avoid any significant seepage not accounted by this simplified model. Results do not show a well-targeted minimum but a zone of lower β_r values. Using a limit of 0.3 for β_r, the top right corner of Figure 6 limited by the blue line corresponds to a narrow range of specific yield (Sy_2=23-30%) and a large range of hydraulic conductivities (K_2=20-10^3 m.d^{-1}). For this range of values, the values of α and β_t remain smaller in absolute values to 0.1 (more precisely α=0.02-0.05 and β_t=0.08-0.1) justifying the approach to first determine K_1 and Sy_1 before looking for constraints on K_2 and Sy_2. Seasonal variations are thus reduced when Sy_2 is significantly increased to 23-30% while the hydraulic conductivity is not limiting as long as it remains larger than 20 m.d^{-1}. Variations are thus reduced thanks to the creation of an upstream aquifer that is sufficiently capacitive to buffer the recharge signal as strongly as possible. Even with the highest values of specific yield, however, β_r does not converge to zero. The upstream aquifer is too far from the piezometer (600 m) to exert a strong influence on the seasonal variations. This and the specific yield values found in the most upper part of possible values for shales indicate that the interface between the geological units might be effectively closer to the piezometer than shown by the geological map.

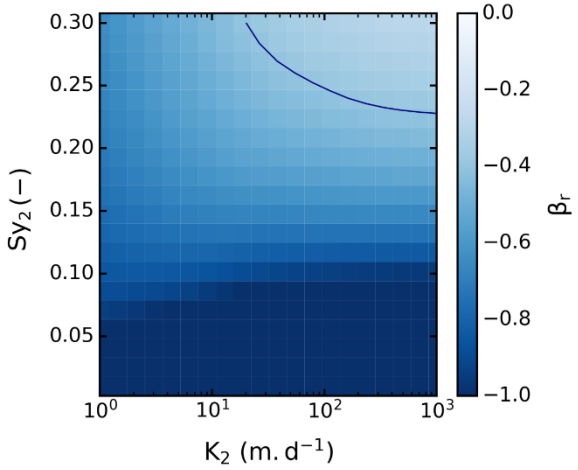

Figure 6: Sensitivity analysis of the β_r criterion as a function of the Brioverian shale hydraulic conductivity K_2 and specific yield Sy_2 (x_i=1000 m).

3.3. Role of the position of the geological interface between the Quaternary sands and Brioverian shales

We repeat the previous method with an interface between Quaternary sands and Brioverian shales no longer at x_i=1000 m but at x_i=500 m to determine to what extent such a configuration would enable a better calibration of the piezometric signal with lower shale specific yield values. K_1 and Sy_1 are kept equal to their previously determined values. β_r is shown as a function of K_2 and Sy_2. It shows a better-defined range of minimal values close to 0. It also leads to smaller specific yields Sy_2 of 10-15 % more in agreement with fractured shales. The hydraulic conductivity K_2 remains poorly defined. The absolute values of α and β_t remain smaller than 0.1 (more precisely α=0.02-0.05 and β_t=0.08-0.1). Even closer to the piezometer, the upstream aquifer has only a minor influence on the average head and tidal fluctuations. It still justifies the approach to first determine K_1 and Sy_1 before looking for constraints on K_2 and Sy_2. Seasonal variations in hydraulic head also suggest that the upstream aquifer is closer than indicated on the geological map (Dupret et al., 1989).

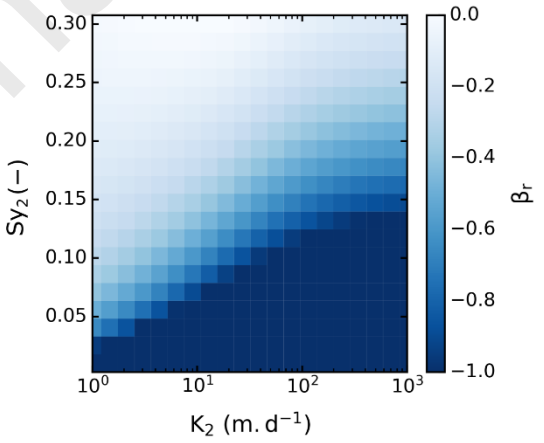

Figure 7: Sensitivity analysis of the β_r criterion as a function of the Brioverian shale hydraulic conductivity K_2 and specific yield Sy_2 (x_i=500 m).

These results are surprising since, first, Quaternary sands are expected to be more porous and permeable than Brioverian shales and second, the lithological interface is indicated further away from the piezometer. Nonetheless, additional information supports the potential existence of highly

permeable formations East of the Quaternary sands. First, several boreholes at the study site show the existence of coarse sands containing pebbles beneath Quaternary eolian sands (Borehole file BSS000KUVT, 2017). Those coarse sands are probably Eemian sands (Dissler et al., 1988; Dupré et al., 1990), potentially extending further East and forming a more capacitive aquifer upstream. Second, a fault was observed and mapped 1.5 km east of the piezometer (Dupret et al., 1987; Rolet et al., 1994), oriented towards it and probably extending in its direction. This fault facilitates hydraulic connection between the low-permeability Brioverian shales and the lower Brioverian formations, which are known to be much more weathered and permeable. The presence of this fault in our study site, extending towards our observation point, could also explain the results indicating a closer interface. Finally, three boreholes drilled in the study area close to the coast show shales at depths averaging 6 m, contributing to explain the lower specific yield in zone 1 (Borehole file BSS000KUVT, 2017). Moreover, hydraulic tests performed in these boreholes give hydraulic conductivities of 7.5 to 22 $m.d^{-1}$ and specific yields of 4 to 15% confirming the ranges of values globally obtained for both formations (Table 2).

4. Effects of spatialization and surface-subsurface interactions

We investigate the specific effects of spatialization and of surface/subsurface interactions on the flow structures and identification process. To this end, we develop a more comprehensive 2D model, identify the hydraulic properties, and determine the similarities and differences with the properties identified in the previous section.

4.1. 2D model characteristics and implementation

The 2D model geometry is extracted from a 25-meter resolution DEM using HydroModPy, a Python toolkit allowing building MODFLOW models from GIS files (Gauvain et al., 2024, in prep.). The modelled area is a rectangular zone of 1 kilometer North-South width, extending 3.3 kilometers East perpendicular to the shoreline (black rectangle, Figure 2). The model has a square mesh configuration, a lateral resolution of 25 meters, and a single layer. Bottom of the model is at the constant elevation of -20 meters. Elevation of the model is ranging from 0 to 25 meters, corresponding to the DEM topography (Figure 1). Flows are computed with MODFLOW NWT using the same initial and boundary conditions as in the previous 1D model case at a daily time step. Initial conditions are defined after running the model in steady state using the mean recharge over the two years preceding the calibration year. Recharge is imposed homogeneously to the whole domain. Seepage is modelled using the DRAIN package (Harbaugh, 2005) and allows water to flow out of the aquifer when hydraulic head intersects topography. We take two assumptions for the location of the interface between Quaternary sand and Brioverian shale hydrogeological zones. The first one is based on the geological map and cross-section (Figure 2) at a distance x_i=1 000 m from the coast. The second one is set closer to the coast at x_i=500 m, based on the previous section findings.

4.2. Hydraulic conductivities as determined by the mean hydraulic head

We first analyze the dependence of the α performance criterion (5) for the original position of the interface (x_i=1000 m) with the Quaternary sands and Brioverian shale hydraulic conductivities K_1 and K_2. Instead of the mean hydraulic head, we use as a proxy the hydraulic head obtained in steady state. Indeed, complementary analyses show only marginal differences of α values between them for the range of K_1 and K_2 values investigated. Results are obtained by an exploration on a 30 by 30 grid of regularly spaced value for K_1 and K_2 taken in the range of values identified by the 1D model (Figure 8). Optimal values of α (white cells) are composed of two sections.

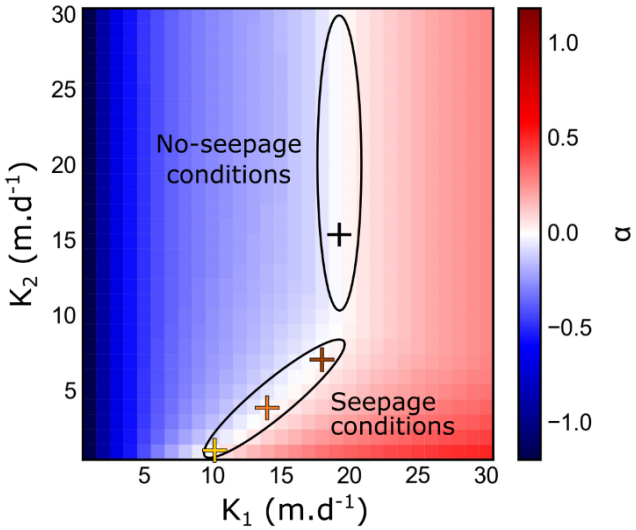

Figure 8: Model to data comparison of steady-state hydraulic heads as measured by α (equation (5)) for the 2D model (x_i=1000 m). Crosses mark the (K_1, K_2) couples for which specific yields will be calibrated with the response to the tidal and seasonal variations: yellow (10 m.d^{-1}, 1 m.d^{-1}), orange (14 m.d^{-1}, 4 m.d^{-1}), brown (17 m.d^{-1}, 6.5 m.d^{-1}), black (18 m.d^{-1}, 15 m.d^{-1}).

The first section of optimal α values is obtained for values of K_1=18 m.d^{-1} and K_2 higher than 8 m.d^{-1}. For those simulations, it has been checked that seepage only occurs marginally in the modelled area. This domain of (K_1, K_2) solutions is thus identified as the "no-seepage conditions" (Figure 8). It matches the solutions obtained for the analytical and 1D numerical models. K_1 is close at 10% to the analytical solution, a good approximation given the coarse resolution of the exploration. K_2 remains unconstrained as long as it is high enough. The steady state piezometric level allows to identify the Quaternary sands hydraulic conductivity K_1.

In the second section identified as the "seepage conditions" (Figure 8), the steady state piezometric level depends not only on the Quaternary sand conductivity K_1 but also on the Brioverian shale conductivity K_2. K_1 values range from 10 to 18 m.d^{-1} and K_2 from 1 to 8 m.d^{-1}. Any reduction in K_1 must be matched by an equivalent reduction in K_2. To keep the same hydraulic head at the observation piezometer, the lower capacity of the Quaternary sands to transmit the incoming flows to the sea should be matched by lesser incoming flows and more seepage in the Brioverian shales. In such cases, the mean hydraulic head constrains a relation between both hydraulic conductivities, which happens to be linear in this case.

A similar pattern is obtained regarding the spatial distribution of α values for the closer interface location (x_i=500 m). In this case, no-seepage conditions are restricted to K_1=22 m.d^{-1} and K_2 higher than 15 m.d^{-1}. The seepage conditions are obtained for lower K_1 values ranging from 5 to 22 m.d^{-1} and K_2 values ranging from 1 to 15 m.d^{-1}. Lower K_1 values are explained by the larger groundwater seepage area occurring in the Brioverian shale zone that is made 500 m wider. Indeed, this extension causes more seepage and thus less water income to the Quaternary sand zone where the piezometer is located. Lower K_1 values are needed to counterbalance this smaller upstream groundwater flow.

4.3. Specific yields as determined by tidal fluctuations and seasonal variations

Simulations are run in transient state to explore the dependence of β_t and β_r with Sy_1 and Sy_2. Hydraulic conductivity K_1 and K_2 are set to their values identified in the previous step at the places identified by crosses in Figure 8.

For the no-seepage conditions in the x_i=1 000 m case, we explore β_t and β_r over a 7 by 7 grid of specific yield values Sy_1 and Sy_2. Results are qualitatively similar to those obtained with the 1D model. β_t remains independent of Sy_2 and leads to Sy_1 value of 8%. For this value of Sy_1, the simulation of the seasonal fluctuations imposes values of Sy_2 in the higher range of values (27-30%) with associated absolute β_r values ranging from 0.42 to 0.46. Comparison with the 1D model (Table 2) shows that the identified values are close at 12 % for Sy_1 and 15 % for Sy_2. In the absence of significant seepage, the 1D model can thus be used for the hydraulic parameter identification.

In the seepage conditions, we analyze the 3 cases marked by the crosses for the x_i=1000 m interface case. As diffusivity of the Quaternary sands has been reported to be conserved in all previous cases (Table 2), we set Sy_1 to keep this same diffusivity (D_1=4.5 10^3 m².d^{-1}). The resulting models still match the tidal fluctuations whatever the investigated values of Sy_2, with β_t remaining lower than 0.28. With Sy_1 respecting this constraint, the seasonal variations remain large whatever the value of Sy_2 ($\beta_r < -0.5$) and even quite larger than in the absence of seepage (Figure 9a). The head variations remain far from the observed ones especially in the recession and flooding periods (Figure 9b). The occurrence of seepage limits even more the reduction of the seasonal variations. This can be explained by a partial disconnection of the upstream and downstream zones by the seepage process, which limits the influence of the hydraulic properties of the Brioverian shales. To counteract this effect, the interface should be positioned even closer to the piezometer than in the no-seepage conditions.

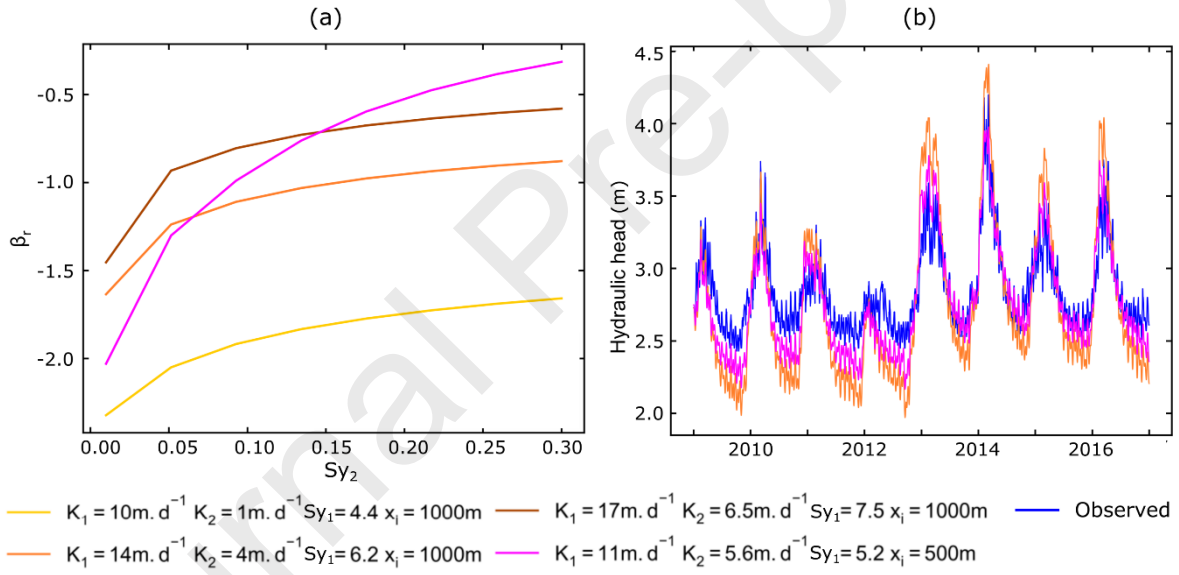

Figure 9: (a) Model to data comparison of the seasonal variations characterized by β_r as a function of the Brioverian shale specific yield Sy_2 for the three cases identified by crosses in Figure 8 within the seepage conditions section. x_i=1000 m (yellow, orange and brown) and x_i=500 m (pink). Quaternary sand specific yield Sy_1 is fixed to keep the diffusivity determined in section 3.1 by the analytical solution. (b) Simulated hydraulic heads obtained for corresponding simulations with Brioverian shale specific yield Sy_2=30%.

The closer interface case (x_i=500 m) gives better results, with β_r values closer to zero (Figure 9a). In this latter configuration, the 3 performance criteria α, β_r and β_t can still be met simultaneously, allowing to represent the main trends of the hydraulic head chronicle (Figure 9b, pink curve). Several types of geological information can explain our hypothesis of a closer interface. As presented by section 3.3, this can be due to lithological variations (Dissler et al., 1988; Dupré et al., 1990) or fault hydraulic connection (Dupret et al., 1987; Rolet et al., 1994). Indeed, the bedrock of the study site is polyphase and abundantly faulted, and uncertainties persist as to the precise characteristics of its depth and nature.

5. Discussion

We propose to synthesize the parameter identification methods previously illustrated on the Gouville hydraulic head chronicle. The aim is to show how these methods can be applied to piezometric signals exhibiting both tidal fluctuations and seasonal variations in cases where (i) heterogeneity occurs between two geological formations separated by an interface globally aligned with the coast and (ii) the topographical gradient does not change much along the coast. The first step is to determine whether the aquifer formation is heterogeneous, by means of a homogeneity test (section 5.1). If heterogeneity is confirmed, the subsequent step is to define an identification method based on approaches that are as accessible as possible without requiring time-consuming calibration operations (section 5.2). We conclude by analyzing the significance of heterogeneity on the coastal vulnerability to groundwater flooding (section 5.3).

5.1. Homogeneity test

The homogeneity test is designed to determine whether the three components of the piezometric signal (mean hydraulic head, tidal fluctuations and seasonal variations) can be obtained simultaneously with a homogeneous model. The test can only be carried out in cases for which the interactions between surface and subsurface are sufficiently limited and do not require advanced spatial representation of the seepage. The test is performed in two steps, based on the decomposition of the piezometric signal into its three components using equations (1), (2), (3) and (4). In the first step, hydraulic conductivity and specific yield are obtained respectively from mean hydraulic head and tidal fluctuations, using the two analytical solutions given by equations (9) and (13). In the second step, a 1D numerical model is developed with these two values of hydraulic conductivity and specific yield. The analytically calibrated model then undergoes a validation procedure, based on available sea-level and recharge data. The simulated seasonal variations are compared with the observed signal using the ratio of their variability given by β_r. If β_r is sufficiently close to 0, the homogeneity test is positive and the hydraulic parameters (conductivity and specific yield) as provided by the two analytical solutions can be applied to the whole domain to simulate hydraulic head variations.

5.2. Identification of the heterogeneous hydraulic properties

When the three components of the piezometric signal cannot be properly simulated using a homogeneous model, the identification method depends on whether seepage is significant. If seepage is not significant, the hydraulic conductivity and specific yield of the geological formation close to the coast can be approximated by their values provided by analytical solutions, based on average head and tide-induced fluctuations. As the hydrodynamic properties determined this way allow proper simulation of mean value and tidal fluctuations of hydraulic head, they can be assigned to the near-shore aquifer formation. The calibration of the seasonal variations (using β_r performance criterion) offers a way to identify some constraints on the hydraulic properties of the far-from-shore aquifer formation. Several identification methods can be used to explore the two-dimensional parameter space formed by its hydraulic conductivity and specific yield. If solutions can effectively be found, it makes sense to get a relationship between properties rather than a single pair of values, since only one constraint is available. In the absence of clear optimal solutions provided by parameter exploration, several causes can be investigated. As for the case presented above, the interface may have been misplaced, making the simulated piezometric signal too insensitive to the far-from-shore geological formation.

Interactions with the surface can impose boundary conditions that limit or, on the contrary, increase seasonal variations. This is especially the case when groundwater seepage occurs. In such cases, the identification method is different since the mean hydraulic head depends on hydraulic conductivity of

both proximal and distal geological formations. Indeed, low upstream hydraulic conductivity values can cause important seepage, leading to reduced downstream heads, which can in turn be counterbalanced by reduced hydraulic conductivity values, as shown in section 4.2. The relation between hydraulic conductivities can be obtained from the average hydraulic head using a transient model or a steady-state model if the steady-state hydraulic head can be shown to be close to the steady-state solution. For each identified valid couple of hydraulic conductivities (providing low α values), the specific yields can be determined by using the tidal and seasonal variations as shown in section 4.3, assuming that their effect on the mean hydraulic head remains limited.

5.3. Seepage areas and vulnerability to aquifer-induced flooding

From a single piezometer data, we infer the possible values of hydraulic conductivity of both Quaternary sands and Brioverian shales. Those values define two main flow regimes, associated to variable groundwater seepage occurrence. In this section, we discuss to what extent our methodology of heterogeneous aquifer property investigation can provide insights on a major issue of some coastal areas that is groundwater-induced flooding. To this end, we use the MODPATH particle tracking module (Pollock, 2016) to analyze the spatial variability of seepage areas. Seepage area location is controlled by time-variant boundary conditions (sea-level, recharge), as well as aquifer properties. Figure 10 shows the resulting flow lines and seepage areas for steady-state simulations using mean observed values of sea-level and recharge rate, and implementing previously inferred values of aquifer properties.

The first simulation (A.) corresponds to the no-seepage conditions (black cross on Figure 8). Associated results show seepage areas only at the shoreline. Groundwater flowlines go straight from the Brioverian foothill to the sea, indicating no surface/subsurface interaction. The second simulation (B.) corresponds to the seepage conditions as defined in section 4.2 (orange cross on Figure 8). Due to the lower hydraulic conductivity K_2, the water table rises up to the surface. While shoreline seepage areas are maintained (with lower rates), additional seepage areas show up along the low-lying points of the sea marsh. Some of the groundwater pathlines end up in these seepage areas, instead of flowing straight to the sea. The third simulation (C.) corresponds to seepage conditions with a lithological interface located at x_i=500 m, i.e. closer to the shoreline. In this configuration, a larger zone of the modelled area is associated to low K_2 values, leading to new seepage areas extending West and reinforcing surface-subsurface interactions.

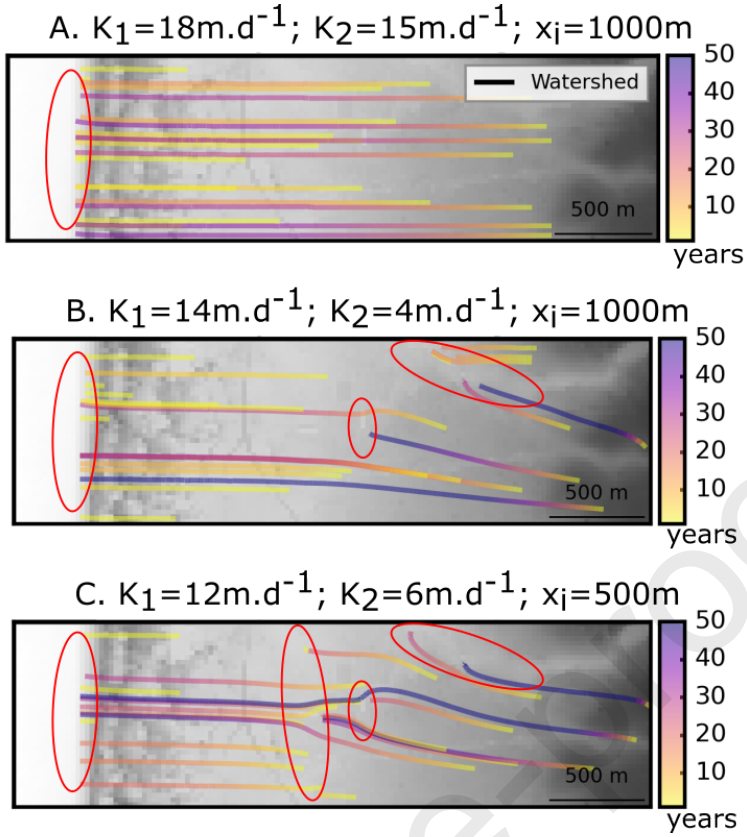

Figure 10: Seepage areas identified by red ellipses and main groundwater time pathlines for different conditions.

Land vulnerability to aquifer-induced flooding can be described as the likelihood of terrains to be part of seepage areas (i.e. to be subject to flooding due to the groundwater rise), or to show high groundwater levels (i.e. having water table at small depths). This analysis shows that a proper identification of hydrodynamic parameter values is necessary to assess this vulnerability. Indeed, if coastal groundwater level is linked to recharge rate, sea level and geomorphology, it is eventually controlled by aquifer hydraulic properties. Our work shows that, in a heterogeneous aquifer made up of two zones, the hydraulic conductivities of both zones control the mean hydraulic head. Hydraulic conductivity controls the capacity of groundwater to drain incoming recharge to the sea and thus its mean level. Low hydraulic conductivity values in the upstream zone can cause important groundwater rise, leading to seepage areas and enhanced vulnerability. In association to hydraulic conductivity, specific yield also impacts land vulnerability, as it controls the amplitude of the water table variations. Lower conductivity increases the water table fluctuations and its probability to generate seepage areas. Close to the shore, lower specific yield values also lead to increased diffusivity and thus to higher tide-induced water table rise (Haehnel et al., 2023).

Identifying hydraulic parameters is essential to assess coastal vulnerability to aquifer saturation and the induced risks on several types of infrastructure, even before reaching the surface. Buildings can crack if water table fluctuations reach swelling clay, and water can rise up the walls by capillary action, producing saltpeter (by bringing minerals from the soil, and drying back) and potentially leading to sanitary issues. Farmlands can also be impacted by groundwater rise, with various effects such as lowered bearing capacity of the soil, or disturbed root systems. Buried networks are also vulnerable to groundwater rise, with damage such as electric wires corrosion, water supply breaking, or groundwater intrusion into sewage networks leading to water treatment plant bypass.

In some cases, analytical and numerical solutions can yield various combinations of hydrodynamic properties, both in terms of values and spatial heterogeneity. In such configurations, seepage areas can be an efficient complementary observation to calibrate the models, as proposed in previous works (Abhervé et al., 2023).

6. Conclusion

We propose a new method for identifying the hydraulic conductivity and specific yield of heterogeneous coastal aquifers using time series of hydraulic heads observed in an isolated piezometer showing clear sensitivity of both marine and continental stresses. The method is based on the interpretation of three components of hydraulic head signal: weekly fluctuations, seasonal variations and multi-year mean levels. In order to calibrate hydraulic conductivity and specific yield values of the two zones that make up the main aquifer terrains, we define new performance criteria. We show that the average hydraulic head depends on the hydraulic conductivity of terrains and on the recharge rate. Weekly fluctuations are essentially determined by the diffusivity of formations between the coast and the piezometer. Seasonal variations are mainly controlled by the hydraulic properties of the upstream zone further away from the coast. In the absence of groundwater seepage, this method uses analytical solutions and numerical models. In the case of significant seepage, more advanced models must be used to separate the effect of heterogeneity from the effect of interactions between surface and subsurface.

Our method fundamentally relies on time-series approaches and multistress analyses to enhance characterization of groundwater systems in coastal areas with limited availability of hydrogeologic information. While other approaches analyze hydraulic response to multiple stresses to better understand groundwater level fluctuations (Bakker and Schaars, 2019; Yang and Mccoy, 2023), we analyze this response to infer some essential information on hydrodynamic properties heterogeneity. Our method can be applied to any coastal site with an observation piezometer sensitive to both continental and marine stresses, and an identified lithological interface defining the heterogeneity location. Depending on the occurrence of surface/subsurface interactions, hydraulic properties can be identified using simplified 1D models or more complex spatialized 2D models. If the data do not allow to fully constrain hydraulic properties, a complementary calibration procedure can be performed using the seepage areas, assuming that they can be identified in the field. Conversely, if head data allow to identify hydraulic properties, seepage areas can be modelled using our method. This approach can have useful applications linked to surface/groundwater interactions in coastal contexts, such as groundwater flooding of low-lying areas or seawater intrusions.

Acknowledgements

This work was supported by the RIVAGES Normands 2100 project to which are contributing the Agence de l'Eau Seine-Normandie, Direction Régionale de l'Environnement, de l'Aménagement et du Logement Normandie, Région Normandie, Communauté de Communes Côte Ouest Centre Manche, Communauté d'Agglomération du Cotentin, Communauté de Communes Coutances Mer et Bocage, Communauté de Communes de la Baie du Cotentin, Communauté Urbaine Caen-la-Mer.

References

Abhervé, R., Roques, C., Gauvain, A., Longuevergne, L., Louaisil, S., Aquilina, L., de Dreuzy, J.R., 2023. Calibration of groundwater seepage against the spatial distribution of the stream network to assess catchment-scale hydraulic properties. Hydrol. Earth Syst. Sci. 27, 3221–3239. https://doi.org/10.5194/hess-27-3221-2023

Aguila, J., McDonnell, M., Flynn, R., Butler, A., Hamill, G., Etsias, G., Benner, E., Donohue, S., 2023. Comparison of saturated hydraulic conductivity estimated by empirical, hydraulic and numerical modeling methods at different scales in a coastal sand aquifer in Northern Ireland. ENVIRONMENTAL EARTH SCIENCES 82. https://doi.org/10.1007/s12665-023-11019-6

Bakker, M., Schaars, F., 2019. Solving Groundwater Flow Problems with Time Series Analysis: You May Not Even Need Another Model. GROUNDWATER 57, 826–833. https://doi.org/10.1111/gwat.12927

Bigot, A., 1897. Sur les dépôts pleistocènes et actuels du littoral de la Basse-Normandie. Comptes Rendus de l'Académie des Sciences, Paris 115.

Carol, E., Kruse, E., Pousa, J., Roig, A., 2009. Determination of heterogeneities in the hydraulic properties of a phreatic aquifer from tidal level fluctuations: a case in Argentina. HYDROGEOLOGY JOURNAL 17, 1727–1732. https://doi.org/10.1007/s10040-009-0478-3

Carr, P., Vanderka, G., 1969. Determining aquifer characteristics by tidal method. Water Resources Research 5, 1023-. https://doi.org/10.1029/WR005i005p01023

Coutard, S., Lautridou, J., Rhodes, E., Clet, M., 2006. Tectonic, eustatic and climatic significance of raised beaches of Val de Saire, Cotentin, Normandy, France. QUATERNARY SCIENCE REVIEWS 25, 595–611. https://doi.org/10.1016/j.quascirev.2005.02.003

Dissler E., Dore F., Dupret L., Gresselin F. & Le Gall J. (1988). L'évolution géodynamique cadomienne du Nord-Est du Massif armoricain. Bull. Soc. géol. France, 8e s., t. IV, pp. 801-814.

Dupret L., Poncet J., Laudridou J.-P., Hommeril P., Lavergne C., Giresse P. & Lamboy M., 1987. Carte géologique de la France à 1/50 000 Coutances.

Dupret L., Poncet J., Laudridou J.-P. & Hommeril P., 1989. Notice explicative de la carte géologique de la France à 1/ 50 000 Coutances, 57 p.

Dupret L., Dissler E., Doré F., Gresselin F. & Le Gall J. (1990). Cadomian geodynamic evolution of the northeastern Armorican Massif (Normandy and Maine). In : D'Lemos R., Strachan R. et Topley C. (Eds.) The Cadomian orogeny. Geol. Soc. London, Sp. Public., vol. 51, pp. 115-131.

Elhaï, H., 1960. A propos des niveaux marins quaternaires en Normandie. Bulletin de la Société Linnéenne de Normandie 1, 137–145.

Ferris, J.G., 1952. Cyclic fluctuations of water level as a basis for determining aquifer transmissibility (Report No. Note 1). Washington, D.C. https://doi.org/10.3133/70133368

Fischer, P., Jardani, A., Krimissa, M., Couegnas, C., 2020. Hydraulic characterization of a highly anthropized coastal aquifer subject to tidal fluctuations. HYDROGEOLOGY JOURNAL 28, 2559–2571. https://doi.org/10.1007/s10040-020-02215-w

Freeze, A., Cherry, J.A., 1979. Groundwater. Prentice Hall.

Gauvain, A., Abhervé, R., Le Mesnil, Martin, Roques, C., Coche, A., Leray, S., Marti, E., Bouchez, C., Aquilina, L., de Dreuzy, J.-R., 2024. HydroModPy: A Python toolkit to automate the deployment of surface-constrained groundwater-flow models at large scale. in preparation.

Gleeson, T., Smith, L., Moosdorf, N., Hartmann, J., Durr, H.H., Manning, A.H., van Beek, L.P.H., Jellinek, A.M., 2011. Mapping permeability over the surface of the Earth. Geophysical Research Letters 38. https://doi.org/10.1029/2010gl045565

Goyetche, T., Pool, M., Carrera, J., Luquot, L., 2022. Hydromechanical characterization of tide-induced head fluctuations in coastal aquifers: The role of delayed yield and minor permeable layers. JOURNAL OF HYDROLOGY 612. https://doi.org/10.1016/j.jhydrol.2022.128128

Habel, S., Fletcher, C., Rotzoll, K., El-Kadi, A., 2017. Development of a model to simulate groundwater inundation induced by sea-level rise and high tides in Honolulu, Hawaii. WATER RESEARCH 114, 122–134. https://doi.org/10.1016/j.watres.2017.02.035

Haehnel, P., Greskowiak, J., Robinson, C., Schuett, M., Massmann, G., 2023. Efficient representation of transient tidal overheight in a coastal groundwater flow model using a phase-averaged tidal boundary condition. ADVANCES IN WATER RESOURCES 181. https://doi.org/10.1016/j.advwatres.2023.104538

Harbaugh, A.W., 2005. MODFLOW-2005 : the U.S. Geological Survey modular ground-water model--the ground-water flow process (Report No. 6-A16), Techniques and Methods. https://doi.org/10.3133/tm6A16

Borehole file BSS000KUVT [WWW Document], 2017. URL http://ficheinfoterre.brgm.fr/InfoterreFiche/ficheBss.action?id=BSS000KUVT (accessed 3.16.24).

Jacob, C., 1950. Flow of groundwater. Engineering hydraulics 321–386.

Jha, M., Namgial, D., Kamii, Y., Peiffer, S., 2008. Hydraulic Parameters of Coastal Aquifer Systems by Direct Methods and an Extended Tide - Aquifer Interaction Technique. WATER RESOURCES MANAGEMENT 22, 1899–1923. https://doi.org/10.1007/s11269-008-9259-3

Knott, J., Elshaer, M., Daniel, J., Jacobs, J., Kirshen, P., 2017. Assessing the Effects of Rising Groundwater from Sea Level Rise on the Service Life of Pavements in Coastal Road Infrastructure. TRANSPORTATION RESEARCH RECORD 1–10. https://doi.org/10.3141/2639-01

Knott, J., Jacobs, J., Daniel, J., Kirshen, P., 2019. Modeling Groundwater Rise Caused by Sea-Level Rise in Coastal New Hampshire. JOURNAL OF COASTAL RESEARCH 35, 143–157. https://doi.org/10.2112/JCOASTRES-D-17-00153.1

Lautridou, J.P., 1989. Les lignes de rivages pléistocènes en Normandie. Âge des plates-formes littorales. Bulletin du Centre de Géomorphologie du CNRS, Caen 36.

Le Moigne, P., Besson, F., Martin, E., Boé, J., Boone, A., Decharme, B., Etchevers, P., Faroux, S., Habets, F., Lafaysse, M., Leroux, D., Rousset-Regimbeau, F., 2020. The latest improvements with SURFEX v8.0 of the Safran–Isba–Modcou hydrometeorological model for France. Geosci. Model Dev. 13, 3925–3946. https://doi.org/10.5194/gmd-13-3925-2020

Li, H., Jiao, J.J., 2003. Influence of the tide on the mean watertable in an unconfined, anisotropic, inhomogeneous coastal aquifer. Advances in Water Resources 26, 9–16. https://doi.org/10.1016/S0309-1708(02)00097-0

Monachesi, L., Guarracino, L., 2011. Exact and approximate analytical solutions of groundwater response to tidal fluctuations in a theoretical inhomogeneous coastal confined aquifer. HYDROGEOLOGY JOURNAL 19, 1443–1449. https://doi.org/10.1007/s10040-011-0761-y

Nielsen, P., 1990. Tidal Dynamics of the water-table in beaches. Water Resources Research 26, 2127–2134. https://doi.org/10.1029/WR026i009p02127

Niswonger, R.G., Panday, S., Ibaraki, M., 2011. MODFLOW-NWT, a Newton formulation for MODFLOW-2005 (Report No. 6-A37), Techniques and Methods. https://doi.org/10.3133/tm6A37

Oude Essink, G.P.; van Baaren, E., and de Louw, P.B., 2010. Effects of climate change on coastal groundwater systems: A modeling study in the Netherlands. Water Resources Research, 46, W00F04.

Pedoja, K., Jara-Muñoz, J., De Gelder, G., Robertson, J., Meschis, M., Fernandez-Blanco, D., Nexer, M., Poprawski, Y., Dugué, O., Delcaillau, B., Bessin, P., Benabdelouahed, M., Authemayou, C., Husson, L., Regard, V., Menier, D., Pinel, B., 2018. Neogene-Quaternary slow coastal uplift of Western Europe through the perspective of sequences of strandlines from the Cotentin Peninsula (Normandy, France). Geomorphology 303, 338–356. https://doi.org/10.1016/j.geomorph.2017.11.021

Richardson, C., Davis, K., Ruiz-González, C., Guimond, J., Michael, H., Paldor, A., Moosdorf, N., Paytan, A., 2024. The impacts of climate change on coastal groundwater. NATURE REVIEWS EARTH & ENVIRONMENT. https://doi.org/10.1038/s43017-023-00500-2

Rignot, E., Velicogna, I., van den Broeke, M., Monaghan, A., Lenaerts, J., 2011. Acceleration of the contribution of the Greenland and Antarctic ice sheets to sea level rise. GEOPHYSICAL RESEARCH LETTERS 38. https://doi.org/10.1029/2011GL046583

Rogers, M., Sukop, M., Obeysekera, J., George, F., 2023. Aquifer parameter estimation using tide-induced water-table fluctuations in the Biscayne Aquifer, Miami-Dade County, Florida (USA). HYDROGEOLOGY JOURNAL. https://doi.org/10.1007/s10040-023-02634-5

Rolet, J., Gresselin, F., Jegouzo, P., Ledru, P. & Wyns, R., 1994. Intracontinental Hercynian Events in the Armorican Massif. In: Chantraine, J., Rolet, J., Santallier, D.S., Piqué, A., Keppie, J.D. (eds) Pre-Mesozoic Geology in France and Related Areas. IGCP-Project 233. Springer, Berlin, Heidelberg. https://doi.org/10.1007/978-3-642-84915-2_20

Rosas, J., Lopez, O., Missimer, T.M., Coulibaly, K.M., Dehwah, A.H.A., Sesler, K., Lujan, L.R., Mantilla, D., 2014. Determination of Hydraulic Conductivity from Grain-Size Distribution for Different Depositional Environments. Groundwater 52, 399–413. https://doi.org/10.1111/gwat.12078

Rotzoll, K., Fletcher, C., 2013. Assessment of groundwater inundation as a consequence of sea-level rise. NATURE CLIMATE CHANGE 3, 477–481. https://doi.org/10.1038/NCLIMATE1725

SHOM, 2020. Références Altimétriques Maritimes. Ports de France métropolitaine et d'outremer. Côtes du zéro hydrographique et niveaux caractéristiques de la marée.

Slooten, L., Carrera, J., Castro, E., Fernandez-Garcia, D., 2010. A sensitivity analysis of tide-induced head fluctuations in coastal aquifers. JOURNAL OF HYDROLOGY 393, 370–380. https://doi.org/10.1016/j.jhydrol.2010.08.032

Winckel, A., Ollagnier, S., Gabillard, S., 2022. Managing groundwater resources using a national reference database: the French ADES concept. SN Applied Sciences 4, 217. https://doi.org/10.1007/s42452-022-05082-0

Yang, G., Mccoy, K., 2023. Modeling groundwater-level responses to multiple stresses using transfer-function models and wavelet analysis in a coastal aquifer system. JOURNAL OF HYDROLOGY 627. https://doi.org/10.1016/j.jhydrol.2023.130426

Yang, H., Tawara, Y., Shimada, J., Kagabu, M., Okumura, A., 2021. Large-scale hydraulic conductivity distribution in an unconfined carbonate aquifer using the ocean tidal propagation. HYDROGEOLOGY JOURNAL 29, 2091–2105. https://doi.org/10.1007/s10040-021-02366-4

Zhang, M., Hao, Y., Zhao, Z., Wang, T., Yang, L., 2021. Estimation of coastal aquifer properties: A review of the tidal method based on theoretical solutions. WILEY INTERDISCIPLINARY REVIEWS-WATER 8. https://doi.org/10.1002/wat2.1498

694

695 We propose a new method for identifying the hydraulic properties of coastal aquifers based on their
696 response to continental and marine influences observed from isolated piezometers displaying both
697 tidal and seasonal fluctuations. From a single piezometer, a first approximation of hydraulic
698 conductivity and porosity can be derived analytically from the mean hydraulic head and its tidal
699 fluctuations. If this approximation also allows a correct simulation of seasonal head variations, the
700 aquifer can be modelled as homogeneous. Otherwise, the seasonal head variations provide constraints
701 on the heterogeneity of hydraulic properties. This new method is applied to a coastal aquifer in
702 Normandy, formed by a relatively flat, kilometer-wide coastal strip of Quaternary sands followed by a
703 foothill of higher Brioverian shales. Hydraulic head variations monitored daily for 8 years in a
704 piezometer located in the Quaternary sand formation enable us to constrain their hydraulic
705 conductivity (5-20 $m.d^{-1}$) and porosity (7-10 %) within restricted ranges. They also suggest the
706 existence of a significantly more porous formation (15-30%) upstream of the observation piezometer,
707 which could consist of more porous sands or fractured shales. In the case of limited surface-subsurface
708 interactions, the identification method relies on a step-by-step combination of analytical solutions and
709 simplified 1D numerical models. When more important surface-subsurface interactions are involved,
710 a spatialized 2D model is used, that allows the analysis of seepage areas. Based on this case study, we
711 gradually introduce 1D and 2D approaches, and discuss their applicability. We finally illustrate one
712 major application of this approach by analyzing the interest of aquifer properties investigation on
713 groundwater-induced flooding vulnerability.

714

715 - Piezometric variations are linked to tidal fluctuations and recharge variations.
716 - Hydraulic conductivity and specific yield calibrated using multistress aquifer response.
717 - Heterogeneous hydraulic properties are identified from an isolated piezometer.
718 - Coastal groundwater flooding vulnerability is assessed using seepage areas analysis.

719

720

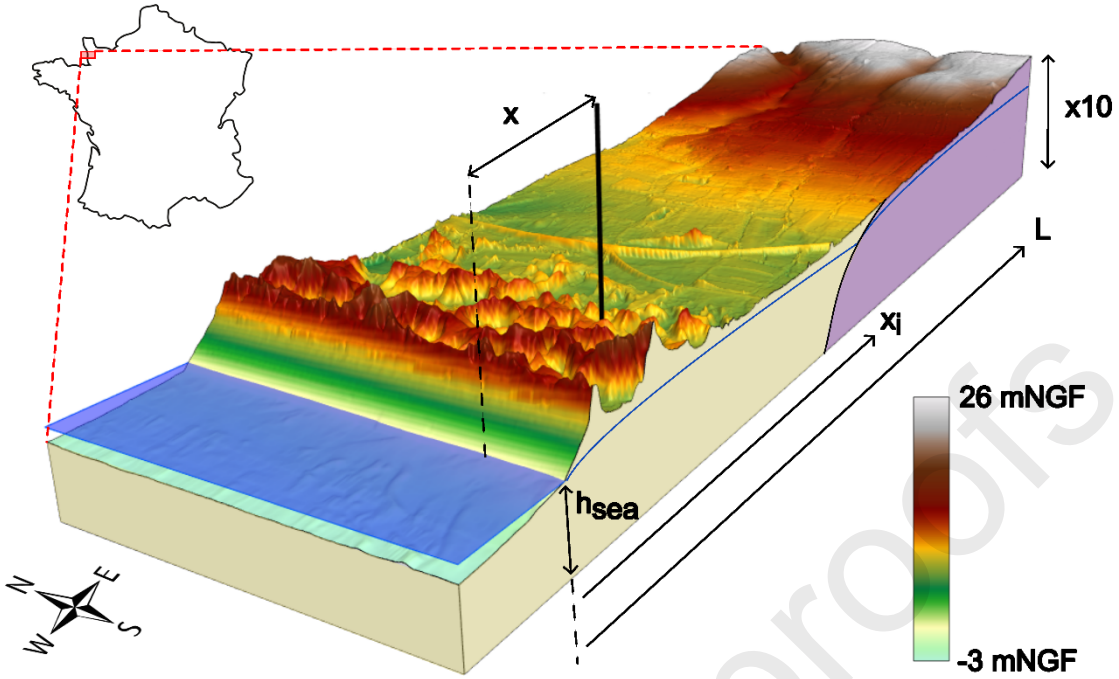

721

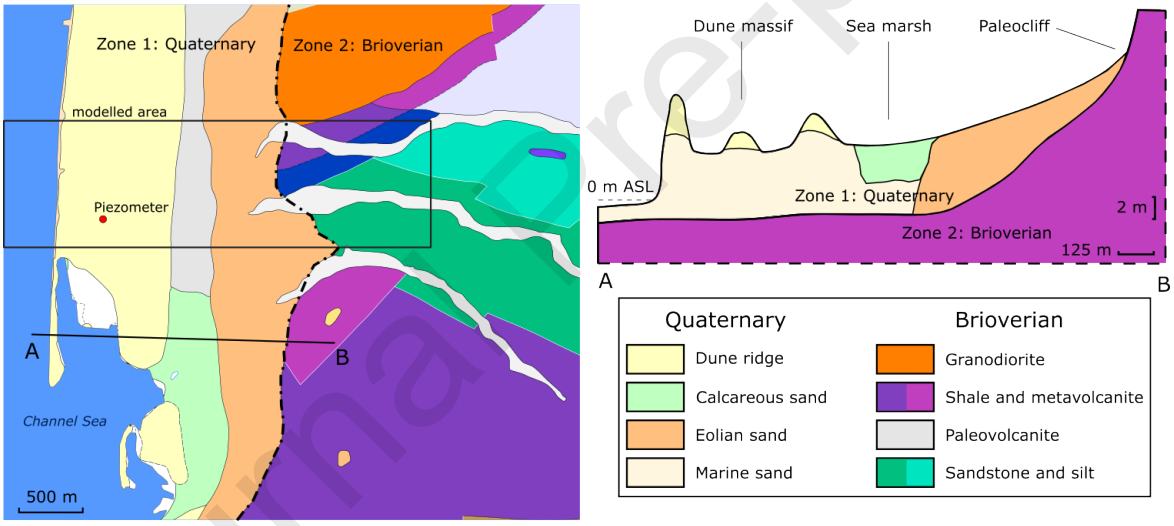

722

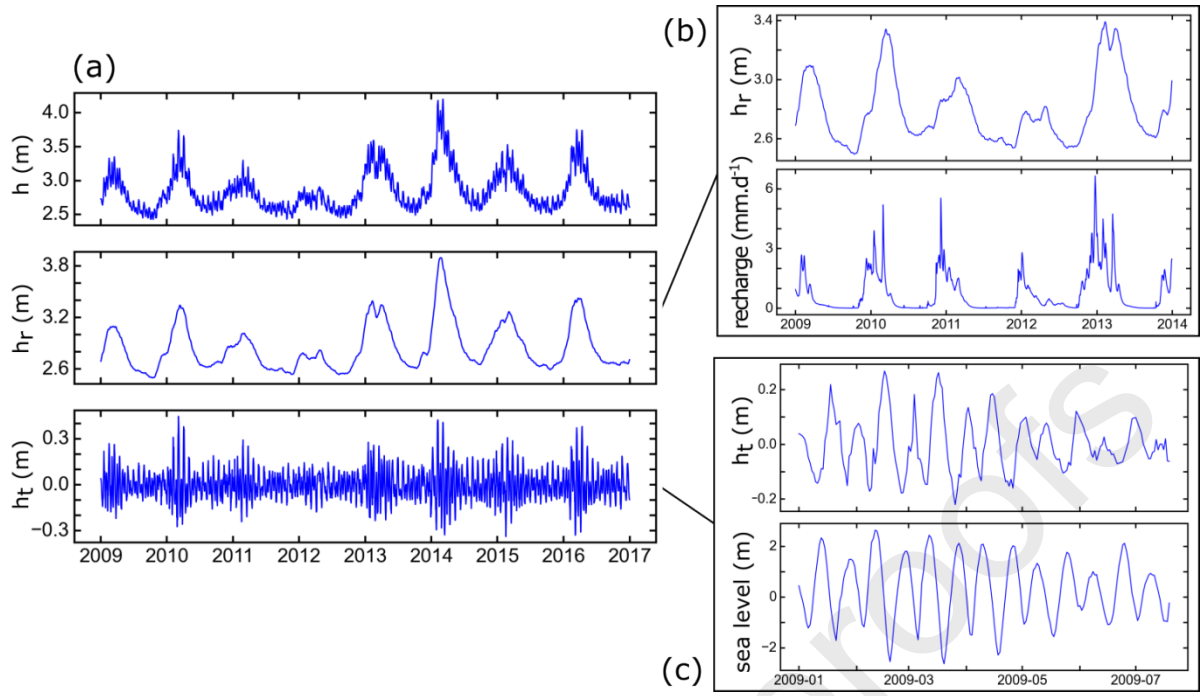

723

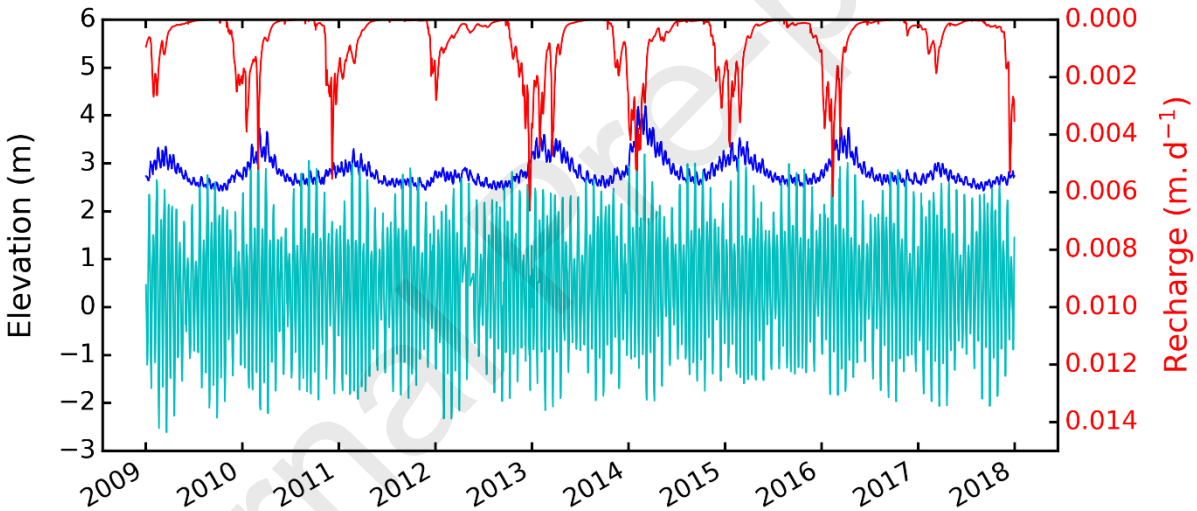

724

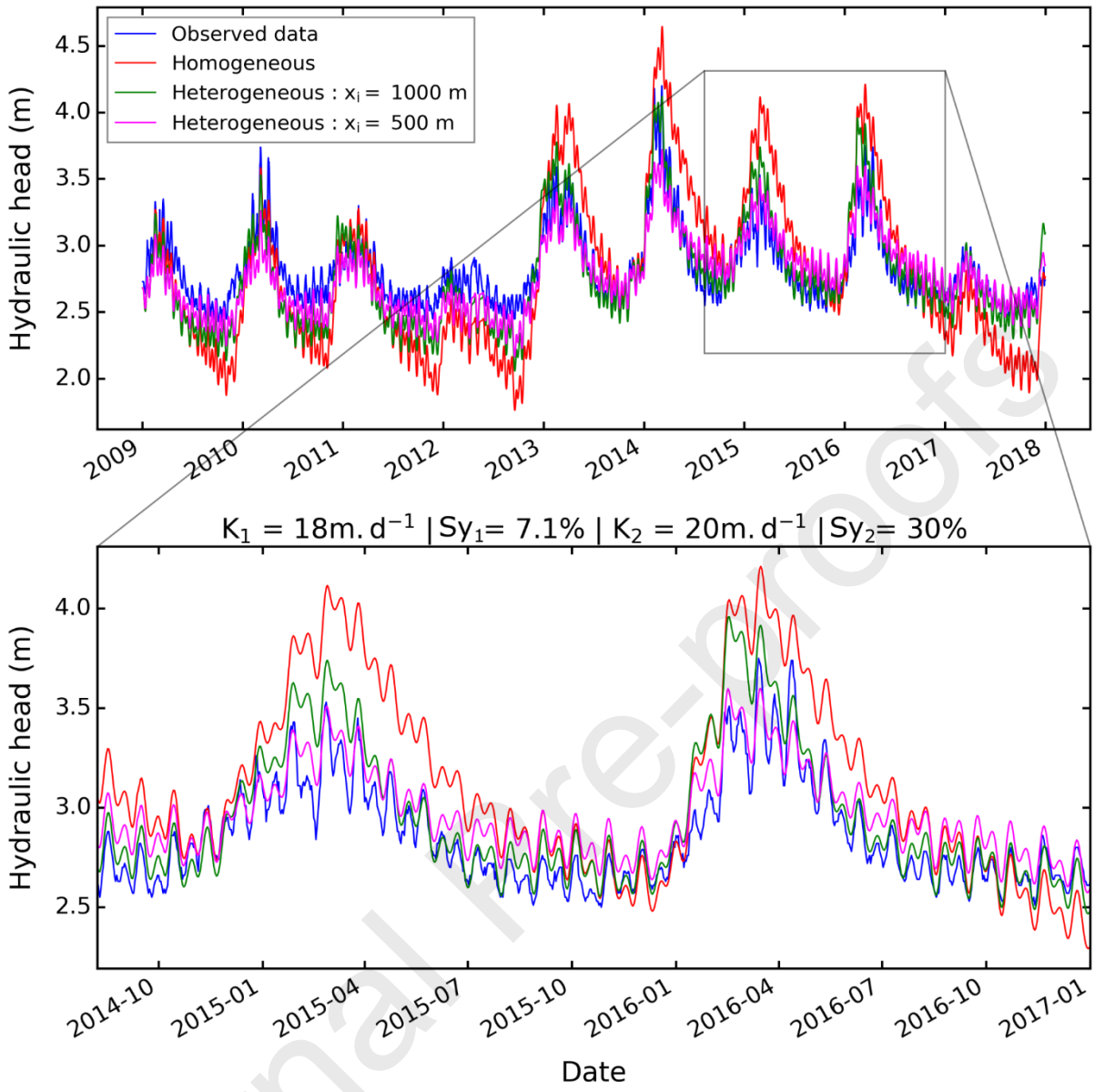

725

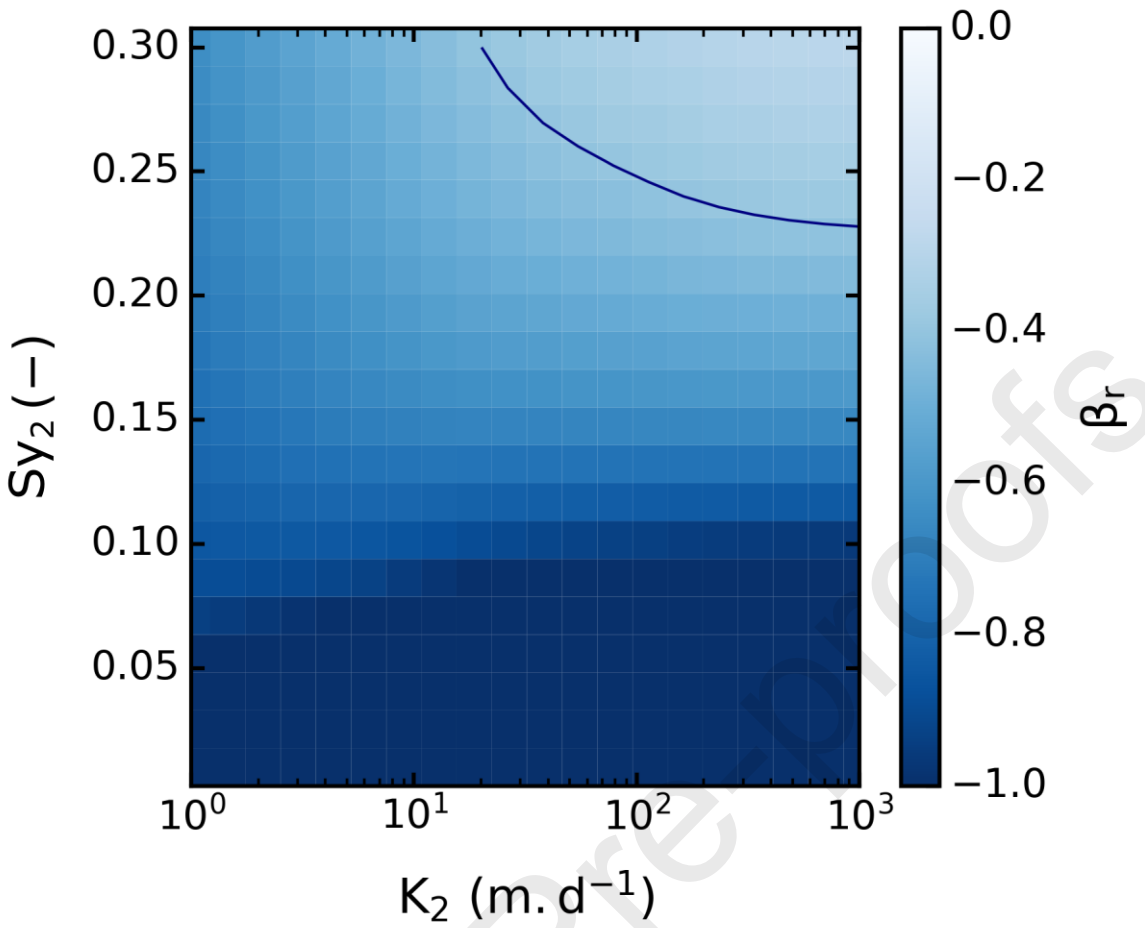

726

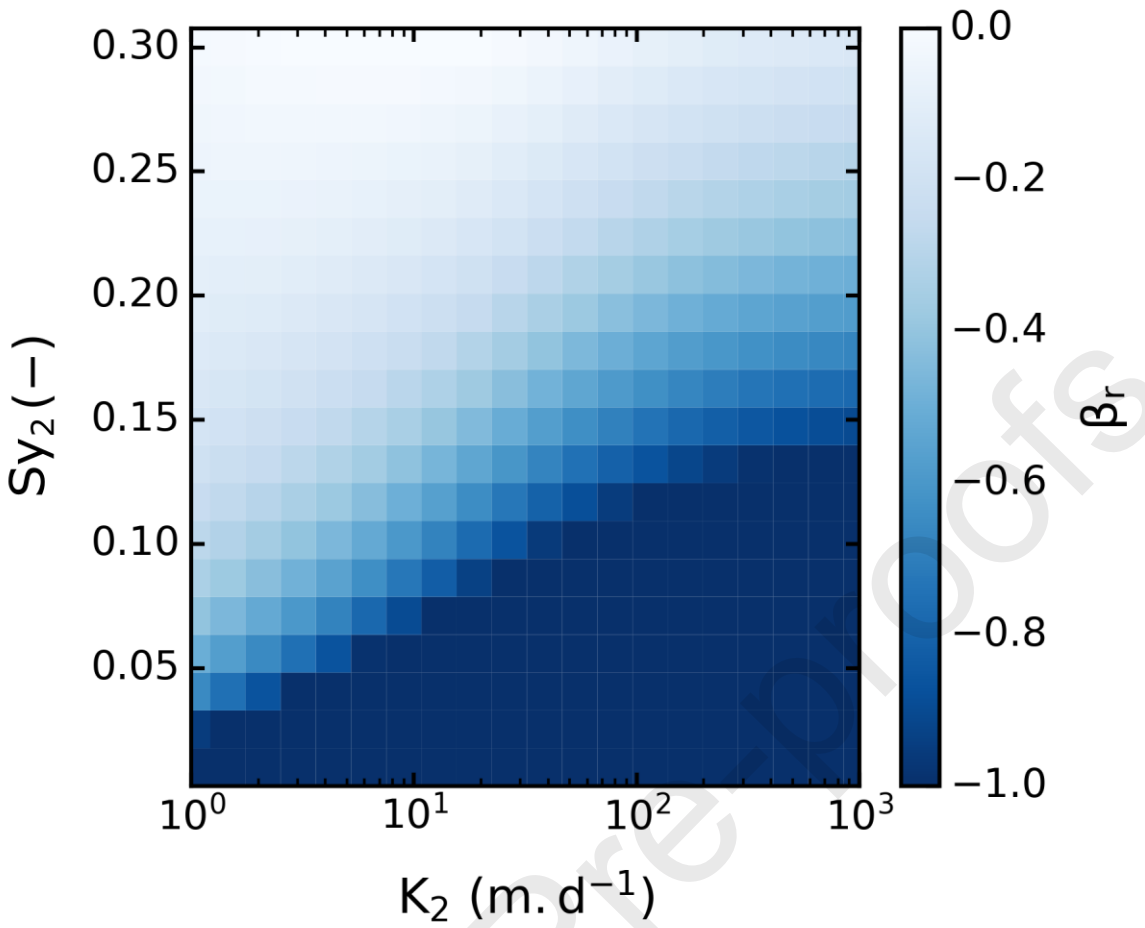

727

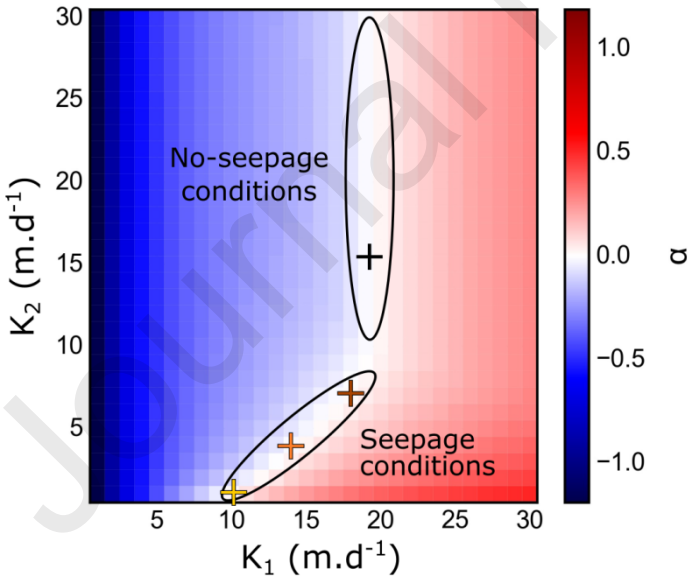

728

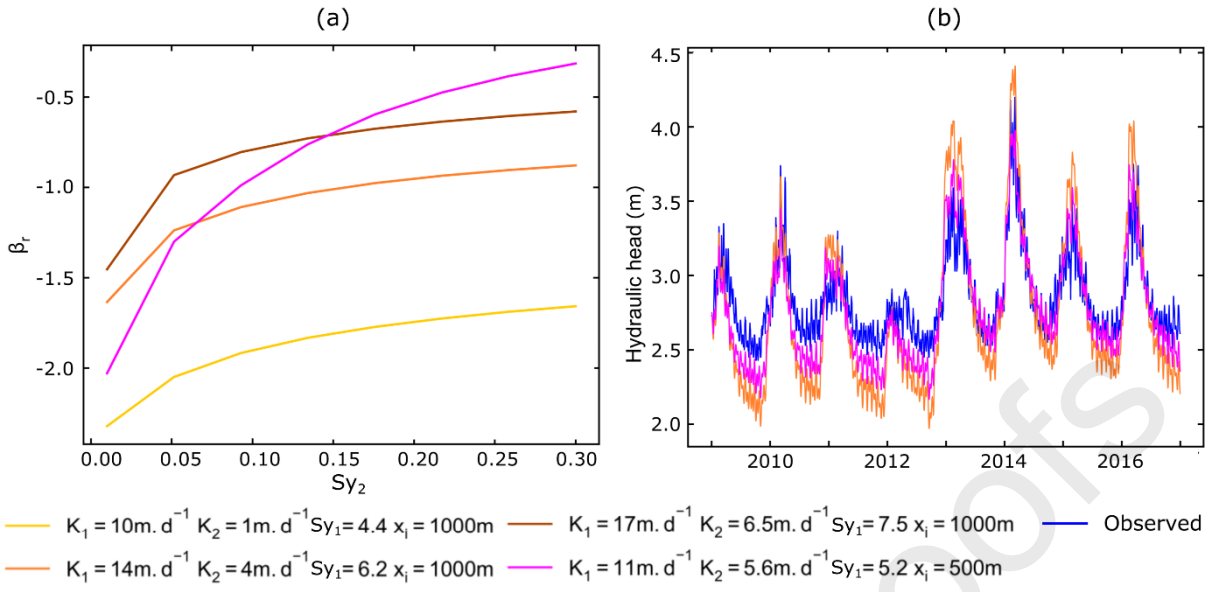

729

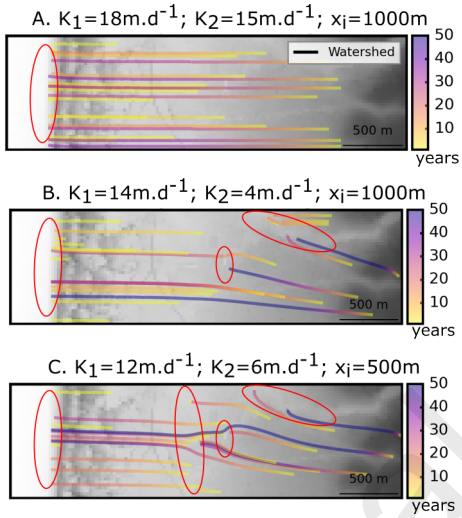

730

Mean aquifer extension	L	3000 m
Distance of the lithological interface to the coast	x_i	600 m
Distance of the piezometer to the coast	X	400 m
Aquifer thickness at the coast	h_{sea}	20 m
Mean recharge rate	R	286 mm.y^{-1}

731

732

	Analytical	**Numerical 1D**	**Numerical 1D**	**Numerical 2D**	**Numerical 2D**	**Numerical 2D**
Distribution	Homogeneous	Homogeneous	Heterogeneous	Heterogeneous	Heterogeneous	Heterogeneous
Seepage	Not allowed	Not allowed	Not allowed	Not observed	Observed	Observed
x_i **(m)**	1 000	1 000	1 000	1 000	1 000	500
K_1 **(m.d^{-1})**	18	18	18	18	10 - 17	5.0 - 20
n_1 **(%)**	10	7.1	7.1	8.0	4.4 – 7.5	4.4 – 7.5
D_1 **(m^2.d^{-1})**	3.5 10^3	5.2 10^3	5.2 10^3	4.5 10^3	2.6 10^3 – 7.7 10^3	1.3 10^3 – 9.0 10^3
K_2 **(m.d^{-1})**			20 – 1.0 10^3	9.0 - 30	1.0 – 8.0	1.0 - 15
n_2 **(%)**			23 - 30	27 - 30	15 – 30	10 - 15
D_2 **(m^2.d^{-1})**			1.3 10^2 – 8.7 10^4	6.0^2 – 2.6 10^3	7.0 10^1 – 7.0 10^2	7.0 10^1 – 1.2 10^3

The authors declare that they have no known competing financial interests or personal relationships that could have appeared to influence the work reported in this paper.